IEEE Access
Multidisciplinary | Rapid Review | Open Access Journal

Received 9 June 2023, accepted 28 June 2023, date of publication 6 July 2023, date of current version 12 July 2023.

Digital Object Identifier 10.1109/ACCESS.2023.3292937

TOPICAL REVIEW

Deterministic Signal Processing Techniques for OFDM-Based Radar Sensing: An Overview

MICHELE MIRABELLA, (Graduate Student Member, IEEE), PASQUALE DI VIESTI, (Graduate Student Member, IEEE), ALESSANDRO DAVOLI, (Graduate Student Member, IEEE), AND GIORGIO M. VITETTA, (Senior Member, IEEE)

Department of Engineering "Enzo Ferrari", University of Modena and Reggio Emilia, 41125 Modena, Italy
Consorzio Nazionale Interuniversitario per le Telecomunicazioni (CNIT), 43124 Parma, Italy

Corresponding author: Michele Mirabella (michele.mirabella@unimore.it)

ABSTRACT In this manuscript, we analyze the most relevant classes of deterministic signal processing methods currently available for the detection and the estimation of multiple targets in a joint communication and sensing system employing orthogonal frequency division multiplexing. Our objective is offering a fair comparison of the available technical options in terms of required computational complexity and accuracy in both range and Doppler estimation. Our numerical results, obtained in various scenarios, evidence that distinct algorithms can achieve a substantially different accuracy-complexity trade-off.

INDEX TERMS Dual-function radar-communication, frequency estimation, harmonic retrieval, joint communication and sensing, maximum likelihood estimation, orthogonal frequency division multiplexing, radar processing, spectral analysis.

I. INTRODUCTION

In the last few years, increasing attention has been paid to the design of wireless systems able to perform both communication and radar functions, i.e. to accomplish joint communication and sensing (JCAS). Such systems make an efficient use of the available spectrum and offer significant benefits in terms of size, energy consumption, and cost, since they employ a single radio device for both communication and sensing functionalities. For these reasons, they are expected to play an important role in the field of future vehicular networks [1], [2], [3].

One of the waveforms currently being considered for its adoption in JCAS systems is orthogonal frequency division multiplexing (OFDM) [4]. A huge technical literature is available about the signal processing techniques to be employed at both the transmit (TX) and receive (RX) sides of wireless communication systems exploiting this modulation format. On the contrary, limited research efforts have been devoted until now to the development of methods for target detection and estimation in OFDM-based JCAS systems. The currently available methods can be divided in *direct sensing methods* and *indirect estimation methods*. The former methods extract target information from the received signal without compensating for the effect of the data payload conveyed by its useful component [5]; moreover, they typically exploit computationally intensive compressed sensing techniques (e.g., see [6], [7], [8], [9]). The latter methods, instead, rely on the knowledge of a preliminary estimate of the communication channel. The evaluation of this estimate requires compensating for the contribution of the transmitted channel symbols to the received signal (such symbols are always known at the receive side of a *colocated* radar; e.g., see [10]). In this manuscript, we focus on indirect methods only and investigate their use in a colocated[1] OFDM-based JCAS system equipped with a single TX and a single RX antenna (i.e., of single-input single-output (SISO) type). Moreover, we take into consideration different classes of indirect methods, namely: 1) discrete Fourier transform (DFT)-based or correlation-based methods; 2) subspace methods; 3) maximum likelihood (ML)

The associate editor coordinating the review of this manuscript and approving it for publication was Li Zhang.

[1] Since the considered system is colocated (i.e., its TX and RX antennas are closely spaced), its receiver has a full knowledge of the structure and content of the transmitted frames and of the carrier frequency.

This work is licensed under a Creative Commons Attribution 4.0 License. For more information, see https://creativecommons.org/licenses/by/4.0/

based methods. It is worth pointing out that, even if various overviews on JCAS systems have appeared in the last three years [4], [5], [11], [12], [13], [14], [15], [16], [17], [18], [19], none of them provides a comparative analysis of the above mentioned methods for sensing in an OFDM-based radar system. Written with the aim of filling this gap, this manuscript offers a fair comparison in terms of accuracy and computational complexity of various algorithms belonging to the aforementioned classes and highlights their peculiarities and limitations.

The remaining part of this manuscript is organized as follows. In Section II, the processing accomplished in an OFDM-based radar system is summarized and the model of the signal feeding target detection and estimation algorithms is illustrated. Section III is devoted to the description of various relevant estimations methods, and to the assessment of their computational complexity. The analyzed techniques are compared in terms of accuracy and complexity in Section IV. Finally, some conclusions are offered in Section V.

Notation: Throughout this paper, $(\cdot)^T$ denotes matrix transposition, whereas $(\cdot)^*$ and $(\cdot)^H$ denote complex conjugate and complex conjugate transpose (Hermitian operator), respectively. Moreover, $\Re\{x\}$ and $\Im\{x\}$ indicate the real and imaginary part, respectively, of the complex variable x. Finally, $\mathbf{0}_{D_1,D_2}$ denotes the $D_1 \times D_2$ null matrix.

II. SYSTEM AND SIGNAL MODELS

In this section, the processing accomplished in a SISO OFDM-based JCAS system is sketched; our main objective is providing the mathematical model of the transmitted signal and of the corresponding received signal in the presence of multiple targets. In our analysis, we focus on the transmission of a single frame, consisting of M consecutive OFDM symbols; the radio frequency (RF) waveform conveying the transmitted frame is (e.g., see [20, eq. (4)])

$$x_{\mathrm{RF}}(t) = \Re\left\{\exp\left(j2\pi f_{\mathrm{c}} t\right) \sum_{m=0}^{M-1} x_m(t)\right\}, \tag{1}$$

where f_{c} denotes the frequency of the local oscillator employed in the TX up-conversion and

$$x_m(t) \triangleq q\left(t - mT_s\right) \sum_{n=0}^{N-1} s_{m,n} \exp\left(j2\pi n\Delta_f \left(t - mT_s\right)\right) \tag{2}$$

is the complex envelope of the transmitted signal conveying the mth OFDM symbol (with $m = 0, 1, \ldots, M-1$); here, $q(t)$ is a *windowing function* (employed for pulse shaping), $s_{m,n}$ is the channel symbol carried by the nth subcarrier of the mth OFDM symbol (with $n = 0, 1, \ldots, N-1$), N is the overall number of subcarriers, $\Delta_f = 1/T$ is the subcarrier spacing, T is the OFDM symbol interval, $T_s \triangleq T + T_G$ is the overall duration of the OFDM symbol and T_G is the *cyclic prefix* duration (also known as *guard time* [10]). In this manuscript, a rectangular windowing function is assumed, so that $q(t) = 1$ for $t \in [-T_G, T]$ and $q(t) = 0$ elsewhere.

Let assume now that $x_{\mathrm{RF}}(t)$ (1) is reflected by K point targets, and that the kth target (with $k = 0, 1, .., K-1$) is located at the (initial) distance R_k from the transmitter and moves at the radial velocity[2] v_k with respect to it. It is not difficult to show that, in this case, the complex envelope of the signal received by the JCAS system is[3]

$$r(t) = \sum_{k=0}^{K-1} A_k \exp\left(j2\pi f_{D_k} t\right) \cdot \sum_{m=0}^{M-1} x_m\left(t - \tau_k + \frac{f_{D_k}}{f_{\mathrm{c}}} t\right) + w(t), \tag{3}$$

where $A_k \triangleq \alpha_k \exp(-j2\pi f_{\mathrm{c}} \tau_k)$ is the complex gain accounting for the attenuation, path loss and phase rotation due to the overall propagation delay $\tau_k \triangleq 2R_k/c$ introduced by the kth target and α_k is a positive parameter accounting for the attenuation and the path loss associated with the same target. Moreover, $f_{D_k} = 2v_k/\lambda$ is the Doppler shift due to the relative velocity of the kth point target with respect to the radar system, $\lambda = c/f_{\mathrm{c}}$ is the wavelength of the radiated signal and $w(t)$ is the complex additive Gaussian noise process affecting $r(t)$. The signal $r(t)$ (3) undergoes analog-to-digital conversion and DFT processing. An analytical model that describes the sequence generated by sampling $r(t)$ in the mth OFDM symbol interval can be obtained as follows. First of all, the right-hand side (RHS) of (2) is substituted in that of (3). Then, extracting the portion associated with the mth OFDM symbol from the resulting expression and substituting t with $t' = t - mT_s$ yields

$$r_m(t') = \sum_{k=0}^{K-1} A_k \exp\left(j2\pi f_{D_k} t'\right) a_m(F_{D_k}) \sum_{n=0}^{N-1} s_{m,n} \cdot a_n(-F_{r_k})\, \xi_n\left(f_{D_k}, t'\right) \zeta_{m,n}\left(f_{D_k}\right) \exp\left(j2\pi n\Delta_f t'\right) + w(t'), \tag{4}$$

$$a_q(F_X) \triangleq \exp(j2\pi q F_X), \tag{5}$$

with q being either m or n if X is either D or r, respectively,

$$F_{r_k} \triangleq \Delta_f\, \tau_k \tag{6}$$

and

$$F_{D_k} \triangleq f_{D_k} T_s \tag{7}$$

are the *normalized target delay* and the *normalized Doppler frequency*,[4] respectively, characterizing the kth target,

$$\xi_n\left(f, t'\right) \triangleq \exp\left(j2\pi n\Delta_f \left(f/f_{\mathrm{c}}\right) t'\right) \tag{8}$$

[2]This velocity is positive (negative) if the target approaches (moves away from) the considered radar system.

[3]In our system, the availability of stable and accurate frequency and timing references is assumed; for this reason, the *time-frequency mismatch* at the RX side is deemed negligible [21, Sec. III-B].

[4]Note that F_{r_k} is always a positive quantity, whereas F_{D_k} is positive (negative) if the kth target is approaching (moving away from) the radar system.

and

$$\zeta_{m,n}(f) \triangleq \left(j2\pi n\Delta_f\,(f/f_c)\,mT_s\right). \tag{9}$$

Sampling $r_m(t')$ (4) at the instant $t'_l \triangleq lT/N$ (that is equivalent to sampling $r(t)$ (3) at the instant $t_l \triangleq t'_l + mT_s$), with $l = 0, 1, \ldots, N-1$, results in

$$r_{m,l} \triangleq r_m(t'_l) = \sum_{k=0}^{K-1} A_k\, D_l\left(f_{D_k}\right) a_m(F_{D_k}) \sum_{n=0}^{N-1} s_{m,n} \cdot a_n(-F_{r_k})\,\xi_{n,l}\left(f_{D_k}\right)\zeta_{m,n}\left(f_{D_k}\right)\exp(j2\pi nl/N) + w_l, \tag{10}$$

where $D_l(f_{D_k}) \triangleq \exp(j2\pi f_{D_k} lT/N)$ accounts for the so-called *range migration* effect due to the kth target Doppler (e.g. see [21]), $\xi_{n,l}(f_{D_k}) \triangleq \xi_n(f_{D_k}, t'_l)$ and $w_l \triangleq w(t'_l)$ is the Gaussian noise affecting $r_{m,l}$ (an additive white Gaussian noise (AWGN) model is assumed for the sequence $\{w_l; l = 0, 1, \ldots, N-1\}$). In the following, we assume that the target Dopplers $\{f_{D_k}\}$ are sufficiently small and, more precisely, $|f_{D_k}/f_c| \ll 1/(MN)$ for any k, so that the factors $\xi_{n,l}(f_{D_k})$ and $\zeta_{m,n}(f_{D_k})$ appearing in the RHS of (10) can be neglected; this leads to the simplified signal model

$$r_{m,l} = \sum_{k=0}^{K-1} A_k\, D_l\left(f_{D_k}\right) a_m(F_{D_k}) \sum_{n=0}^{N-1} s_{m,n} \cdot a_n(-F_{r_k})\exp(j2\pi nl/N) + w_l. \tag{11}$$

The N signal samples acquired in the mth OFDM symbol interval undergo *serial-to-parallel* (S/P) conversion; this produces the N-dimensional vector $\mathbf{r}_m \triangleq [r_{m,0}, r_{m,1}, \ldots, r_{m,N-1}]^T$ for which an order N DFT is computed. The nth element of the resulting DFT output vector

$$\mathbf{R}_m \triangleq [R_{m,0}, R_{m,1}, \ldots, R_{m,N-1}]^T, \tag{12}$$

can be expressed as

$$R_{m,n} = s_{m,n} \sum_{k=0}^{K-1} A_k a_m(F_{D_k}) a_n(-F_{\rho_k}) + W_{m,n}, \tag{13}$$

where $W_{m,n}$ is the Gaussian noise affecting the nth subcarrier of the mth OFDM symbol and

$$F_{\rho_k} = F_{r_k} - F_{D_k} T/(NT_s) \tag{14}$$

is a normalized frequency accounting for the target delay and the range migration due to its velocity. In the following we assume that N is large enough, so that the $F_{\rho_k} \approx F_{r_k}$ for any k, thus (13) can be simplified as

$$R_{m,n} = s_{m,n} \sum_{k=0}^{K-1} A_k\, a_m(F_{D_k})\, a_n(-F_{r_k}) + W_{m,n}. \tag{15}$$

Since the channel symbol $s_{m,n}$ is known at the receive side for any n and m, the estimate

$$\hat{H}_{m,n} \triangleq \frac{R_{m,n}}{s_{m,n}} \triangleq \sum_{k=0}^{K-1} A_k\, a_m(F_{D_k})\, a_n(-F_{r_k}) + \bar{W}_{m,n} \tag{16}$$

of the channel gain $H_{m,n}$ observed at the nth subcarrier frequency in the mth OFDM symbol interval can be computed; here,

$$\bar{W}_{m,n} \triangleq \frac{W_{m,n}}{s_{m,n}} \tag{17}$$

is the noise sample affecting $\hat{H}_{m,n}$, in (16). It is worth pointing out that:

1) The parameters F_r (6) and F_D (7) satisfy the inequalities $F_{r,\min} \leqslant F_r \leqslant F_{r,\max}$ and $F_{D,\min} \leqslant F_D \leqslant F_{D,\max}$, with $F_{r,\min} = 0$, $F_{r,\max} = 1$ and $F_{D,\min} = -1/2$, $F_{D,\max} = 1/2$, respectively.

2) an AWGN model is adopted for the noise samples $\{W_{m,n}\}$ (see (15)) and, consequently, for the noise samples $\{\bar{W}_{m,n}\}$ (see (17)), since a phase shift keying (PSK) constellation is employed in our simulations (each element of the sequence $\{\bar{W}_{m,n}\}$ is assumed to have zero mean and variance $\sigma^2_{\bar{W}}$).

3) Neglecting self-interference and range migration results in a signal model in which the target delay and Doppler frequency are decoupled parameters. This entails that, in principle, the values of these parameters can be evaluated separately through 1D frequency estimation techniques. However, only 2D frequency estimation techniques are considered in the following since, despite their higher computational effort than their 1D counterparts, they achieve better accuracy and do not require the use of a pairing method to associate the estimated delays and Doppler frequencies with each detected target.

4) Even if clutter plays an important role in radar sensing, its contribution to the received signal can be mitigated resorting to various techniques available in the technical literature (e.g., see [6]). For this reason, in our work, this contribution is always neglected.

From (16) it can be easily inferred that: a) the noisy samples $\{\hat{H}_{m,n}\}$ of the two-dimensional (2D) channel response acquired over a single frame can be modelled as the superposition of multiple 2D complex exponentials with AWGN; b) target detection and estimation is tantamount to identifying the K complex exponentials forming the useful component of the 2D sequence $\{\hat{H}_{m,n}\}$ and at estimating their parameters, respectively.

III. DETECTION AND ESTIMATION ALGORITHMS

In this subsection, various algorithms for the detection and estimation of multiple targets in an OFDM-based radar systems are illustrated and their computational complexity is analyzed by deriving the order of magnitude of the number of *floating point operations* (FLOPs) they require to process a single OFDM frame. The general criteria adopted in estimating the computational cost of the various algorithms are the same as those illustrated in [22] and [23, Appendix C]. These algorithms are divided in FFT-based techniques, subspace-based methods and ML-based techniques.

A. FFT-BASED TECHNIQUES

Correlation-based and DFT-based methods have been developed in [24], [25], [26], [27], [28], [29], [30], [31], and [32]. In particular, matched filter (MF)-based techniques for the estimation of range and Doppler in a single or multi-target scenario have been investigated in [24] and [32]. Such techniques benefit from the prior knowledge of the received signal and are computationally efficient; however, the accuracy they achieve in radar imaging may be poor because of high sidelobes and leakage, especially in the presence of strong clutter around real targets. A serial cancellation technique for improving the overall accuracy of radar images has been developed in [33], whereas a reduced complexity method, based on the idea of splitting a 2D estimation problem (involving target range and Doppler) into a couple of one-dimensional (1D) simpler sub-problems, has been illustrated in [29].

In the following we take into consideration the 2D *periodogram method* (dubbed 2D-FFT in the following) and two cancellation-based estimation algorithms, namely the *complex single frequency delay estimation and cancellation* (CSFDEC) algorithm [33] and the CLEAN algorithm [34], [35]. On the one hand, the first algorithm can be considered as a reference technique; on the other hand, the other two algorithms as methods able to efficiently mitigate the main problems of the first one, namely: 1) the limited accuracy due to the discretization of the grid selected in the search for the peaks of the periodogram; 2) the need to search for multiple local maxima, which can lead to missed target detection in the presence of closely spaced targets; 3) the significant impact that spectral leakage may have in the presence of multiple targets. In fact, both the CSFDEC and the CLEAN algorithms combine the serial cancellation of the spectral contribution of each detected target with leakage compensation and re-estimation techniques. Moreover, unlike the 2D-FFT algorithm, they do not need a prior knowledge of the overall number of targets.[5]

1) TWO-DIMENSIONAL PERIODOGRAM METHOD

This method is based on the so-called *range-Doppler* map [26], i.e. on the function

$$J[l,p] = |S[l,p]|^2, \tag{18}$$

with $l = 0, 1, \ldots, M_0 - 1$ and $p = 0, 1, \ldots, N_0 - 1$; here,

$$S[l,p] \triangleq \frac{1}{MN} \sum_{m=0}^{M-1} \sum_{n=0}^{N-1} \hat{H}_{m,n}\, a_m(-F_D[l])\, a_n(F_r[p]), \tag{19}$$

is the coefficient (l,p) of the order (M_0, N_0) discrete symplectic Fourier transform (DSFT) of the 2D sequence $\{\hat{H}_{m,n}\}$.

[5]This is a relevant feature of all the detection and estimation algorithms that exploit a serial cancellation procedure for the sequential detection of multiple targets.

Moreover,

$$F_D[l] \triangleq l/M_0 - 1/2, \tag{20}$$

$$F_r[p] \triangleq p/N_0, \tag{21}$$

$$M_0 \triangleq L_D M, \tag{22}$$

$$N_0 \triangleq L_r N; \tag{23}$$

and L_D and L_r are the *oversampling factors* adopted in the Doppler and range domain, respectively. The estimates of the normalized Doppler frequency F_D and the normalized delay F_r of a single target are evaluated as $\hat{F}_D = F_D[\hat{l}]$ and $\hat{F}_r = F_r[\hat{p}]$, respectively, where

$$(\hat{l}, \hat{p}) \triangleq \arg \max_{\tilde{l} \in \mathcal{S}_{M_0}, \tilde{p} \in \mathcal{S}_{N_0}} J[\tilde{l}, \tilde{p}] \tag{24}$$

and $\mathcal{S}_X$ is the set of integers $\{0, 1, \ldots, X-1\}$ for any positive integer X. Given $\hat{l}$ and $\hat{p}$, the target complex amplitude A is estimated as

$$\hat{A} = L_D\, L_r\, S[\hat{l}, \hat{p}]. \tag{25}$$

In a multi-target scenario, multiple (say $\hat{K}$, where $\hat{K}$ denotes a prior estimate of the number of targets K) local maxima[6] should be expected in the *range-Doppler* map; in this case, the parameters of the target associated with each local maximum are evaluated according to (20), (21) and (25).

The most computationally intensive task required by this method is represented by the evaluation of the above mentioned order (M_0, N_0) DSFT (see (19)). Then, the cost for the search of $\hat{K}$ local maxima in the range-Doppler map has to be added to the previous cost. For this reason, the overall computational cost of the 2D-FFT method is $\mathcal{C}_{\text{2D-FFT}} = \mathcal{O}(N_{\text{2D-FFT}})$, where

$$N_{\text{2D-FFT}} = M_0\, N_0\, \log_2(M_0 N_0) + \hat{K}(M_0 N_0). \tag{26}$$

2) CLEAN ALGORITHM

The use of the CLEAN algorithm in radar systems has been proposed in [34], [35], and [36]. On the one hand, one of the earliest implementations of the CLEAN algorithm can be found in [34], where the cancellation capability of the CLEAN algorithm is adopted to reduce sidelobe-induced artifacts affecting the images generated by microwave systems that employ antenna arrays. On the other hand, a more recent CLEAN-based algorithm has been proposed in [35] and [36], where it is employed in the context of stepped frequency continuous wave (SFCW) radar technology. In that case, the algorithm also includes a technique for the compensation of the spectral leakage due to close targets. In this subsection, we show how this algorithm can be also employed for jointly estimating the range and velocity of multiple targets in the OFDM-based radar system described in the previous section. The CLEAN algorithm is based on the same cost function as the 2D-FFT method (see (18)), but, unlike it, makes use

[6]In our simulations, the *Fast* 2D *peak finder* function available in MatlabR2022a has been exploited to locate all the relevant peaks in range-Doppler maps.

of an iterative target cancellation procedure. This means that, within each of its iterations, after detecting a new target and estimating its parameters, its contribution to the above mentioned cost function is cancelled; this results in a *residual* cost function, which is passed to the next iteration. More precisely, the processing executed by the CLEAN algorithm consists in an initialization step followed by an iterative procedure. In the initialization, we set the iteration index k to 0 and

$$\hat{H}_{m,n}[0] = \hat{H}_{m,n}, \tag{27}$$

with $m = 0, 1, \ldots, M-1$ and $n = 0, 1, \ldots, N-1$. Then, in the kth iteration (with $k = 0, 1, \ldots, \hat{K}-1$, where $\hat{K}$ denotes the overall number of detected targets), the four steps described below are carried out sequentially.

1) *Computation of the cost function* — The cost function

$$J_k[l,p] = |S_k[l,p]|^2 \tag{28}$$

is computed for $l = 0, 1, \ldots, M_0-1$ and $p = 0, 1, \ldots, N_0-1$; here, $S_k[l,p]$ is expressed by (19), where, however, $\hat{H}_{m,n}$ is replaced by $\hat{H}_{m,n}[k]$ (see (29) below).

2) *Estimation of the parameters of a new target* — A search for the global maximum over the set $\{J_k[l,p];\ l \in \mathcal{S}_{M_0},\ p \in \mathcal{S}_{N_0}\}$ (collecting $M_0 N_0$ values) is performed to detect a new target (i.e., the kth target); the value of the couple (l,p) corresponding to the global maximum is denoted $(\hat{l}_k, \hat{p}_k)$. Then, the estimates of the normalized frequency F_{D_k} and of the normalized delay F_{r_k} of the kth target are evaluated as $\hat{F}_{D_k} = F_D[\hat{l}_k]$ and $\hat{F}_{r_k} = F_r[\hat{p}_k]$, respectively (see (20) and (21)); whereas that of its complex amplitude $\hat{A}_k$ is evaluated according to (25), where $S[\hat{l},\hat{p}]$ is replaced by $S_k[\hat{l}_k,\hat{p}_k]$.

3) *Threshold test to identify false targets* — If $|\hat{A}_k| < \mathcal{T}_{\text{CLEAN}}$, where $\mathcal{T}_{\text{CLEAN}}$ denotes a proper (positive) threshold, a false target is identified and the execution is stopped by moving to step 5); otherwise, we proceed with the next step.

4) *Target cancellation* — The new residual frequency response

$$\hat{H}_{m,n}[k+1] \triangleq \hat{H}_{m,n}[k] - \hat{A}_k\, a_m\big(\hat{F}_{D_k}\big)\, a_n\big(-\hat{F}_{r_k}\big) \tag{29}$$

is evaluated to cancel the contribution of the last detected target to $\hat{H}_{m,n}[k]$ (with $m = 0, 1, \ldots, M-1$ and $n = 0, 1, \ldots, N-1$). Then, the iteration index k is increased by one and a new iteration is started (i.e., we go back to step 1)).

5) *End* — The final output provided by the CLEAN algorithm is represented by the set $\{(\hat{F}_{D_k}, \hat{F}_{r_k}, \hat{A}_k);\ k = 0, 1, \ldots, \hat{K}-1\}$, where $\hat{K}$ represents the last value taken on by the iteration index k.

The serial cancellation procedure expressed by eq. (29) may suffer from *error accumulation*, since the effects of errors in the estimation of target parameters accumulate over successive iterations. This may result in: a) poor accuracy in the presence of multiple and/or closely spaced targets; b) the detection of false targets. These considerations motivate the use of a *refinement procedure* to be accomplished after the last iteration of the CLEAN algorithm. This procedure consists of N_{REF} iterations. In its ith iteration (with $i = 1, 2, \ldots, N_{\text{REF}}$), the refined estimates $\{(\hat{F}_{D_k}^{(i)}, \hat{F}_{r_k}^{(i)}, \hat{A}_k^{(i)});\ k = 0, 1, \ldots, \hat{K}-1\}$ of the parameters of the $\hat{K}$ targets detected by the CLEAN algorithm are evaluated as follows. First of all, we maximize, over a specific *rectangular grid* (consisting of $\tilde{M}_0 \tilde{N}_0$ distinct nodes), the function

$$J_k^{(i)}\big(\tilde{F}_D, \tilde{F}_r\big) = \Big|S_k^{(i)}\big(\tilde{F}_D, \tilde{F}_r\big)\Big|^2, \tag{30}$$

where

$$S_k^{(i)}\big(\tilde{F}_D, \tilde{F}_r\big) \triangleq \frac{1}{MN} \sum_{m=0}^{M-1} \sum_{n=0}^{N-1} \hat{H}_{m,n}^{(i)}[k]\, a_m\big(-\tilde{F}_D\big)\, a_n\big(\tilde{F}_r\big) \tag{31}$$

and

$$\hat{H}_{m,n}^{(i)}[k] = \hat{H}_{m,n}[0] - \sum_{j=0,\, j\neq k}^{\hat{K}-1} \hat{A}_j^{(i-1)} a_m\big(\hat{F}_{D_j}^{(i-1)}\big)\, a_n\big(-\hat{F}_{r_j}^{(i-1)}\big), \tag{32}$$

with $k = 0, 1, \ldots, \hat{K}-1$. The above mentioned grid, that has a significant impact on the accuracy achieved by the CLEAN algorithm, has the following properties: 1) its center depends on both $\hat{F}_{D_k}^{(i-1)}$ and $\hat{F}_{r_k}^{(i-1)}$; 2) its step sizes get smaller as i increases. More precisely, its node (z_D, z_r) (with $z_D = 0, 1, \ldots, \tilde{M}_0-1$ and $z_r = 0, 1, \ldots, \tilde{N}_0-1$) is associated with the frequencies $(\tilde{F}_D^{(i)}[z_D], \tilde{F}_r^{(i)}[z_r])$.[7] In Table 1 it is shown how the nodes of the above mentioned grid are selected; in that Table, $\delta_X = 1/M_0$ and $\tilde{Q}_0 = \tilde{M}_0 - 1$ if $X = D$ ($\delta_X = 1/N_0$ and $\tilde{Q}_0 = \tilde{N}_0 - 1$ if $X = r$). The nodes are grouped in the set

$$\mathcal{I}_{D,r}^{(i)}\big(\tilde{M}_0, \tilde{N}_0\big) = \mathcal{I}_D^{(i)}\big(\tilde{M}_0\big) \times \mathcal{I}_r^{(i)}\big(\tilde{N}_0\big), \tag{36}$$

where $\times$ denotes the Cartesian product between two sets, $\mathcal{I}_D^{(i)}(\tilde{M}_0)$ and $\mathcal{I}_r^{(i)}(\tilde{N}_0)$ are the sets collecting the $\tilde{M}_0$ and $\tilde{N}_0$ frequencies $\{\tilde{F}_D^{(i)}[z_D]\}$ and $\{\tilde{F}_r^{(i)}[z_r]\}$, respectively.

Maximizing the function $S_k^{(i)}(\tilde{F}_D, \tilde{F}_r)$ (31) over $\mathcal{I}_{D,r}^{(i)}$ (36) leads to the estimates $\hat{F}_{D_k}^{(i)}$ and $\hat{F}_{r_k}^{(i)}$ of F_{D_k} and F_{r_k}, respectively. Finally, the new estimate $\hat{A}_k^{(i)} = S_k^{(i)}(\hat{F}_{D_k}^{(i)}, \hat{F}_{r_k}^{(i)})$ of A_k is evaluated.

It is important to point out that: 1) the evaluation of $\hat{H}_{m,n}^{(i)}[k]$ according to (32) aims at cancelling the contribution given to $\hat{H}_{m,n}[0]$ by the $(\hat{K}-1)$ targets different from the kth one in the ith iteration; 2) at the end of the last (i.e., of the N_{REF}th) iteration, the refined estimates $\{(\hat{F}_{D_k}^{(N_{\text{REF}})}, \hat{F}_{r_k}^{(N_{\text{REF}})}, \hat{A}_k^{(N_{\text{REF}})});\ k = 0, 1, \ldots, \hat{K}-1\}$ become available; 3) the value assigned to δ_X (with $X = D$ and r) allows to cover two adjacent bins of the evaluated DSFT.

It can be shown that the computational cost of the CLEAN algorithm with refinement is $\mathcal{O}(N_{\text{CL}})$, where (see [36, Sec. III-E, eq. (43)])

$$N_{\text{CL}} = \bar{N}_{\text{CL}}(M_0, N_0) + N_{\text{REF}}\, \bar{N}_{\text{CL}}\big(\tilde{M}_0, \tilde{N}_0\big). \tag{37}$$

[7] In the equations listed in Table 1 and in (36), the dependence of $\tilde{F}_X^{(i)}[z_X]$ and $\mathcal{I}_{D,r}^{(i)}$ on the target index k is not specified to ease notation.

TABLE 1. Description of the grid employed for the refinement step of the CLEAN algorithm.

Condition	Grid nodes	Eq.
$F_{X,\min} \leqslant \hat{F}_{X_k}^{(i-1)} < F_{X,\min} + \delta_X$	$\tilde{F}_X^{(i)}[z_X] = F_{X,\min} + (z_X/\tilde{Q}_0)\,(\delta_X/i)$	(33)
$F_{X,\min} + \delta_X \leqslant \hat{F}_{X_k}^{(i-1)} \leqslant F_{X,\max} - \delta_X$	$\tilde{F}_X^{(i)}[z_X] = \hat{F}_{X_k}^{(i-1)} + ((z_X/\tilde{Q}_0) - 1/2)(\delta_X/i)$	(34)
$F_{X,\max} - \delta_X < \hat{F}_{X_k}^{(i-1)} \leqslant F_{X,\max}$	$\tilde{F}_X^{(i)}[z_X] = F_{X,\max} + ((z_X/\tilde{Q}_0) - 1)(\delta_X/i)$	(35)

Here,

$$\bar{N}_{\mathrm{CL}}(M_0, N_0) = K[MN\,(6M_0N_0 + 15) + 2M_0N_0\,(M+N)] \tag{38}$$

is the contribution due a single iteration of the algorithm; note that the parameters (M_0, N_0) and $(\tilde{M}_0, \tilde{N}_0)$ define the grid sizes for the initialization and for the refinement steps, respectively.

3) CSFDEC ALGORITHM

The CSFDEC algorithm, developed in [33], combines a single 2D tone estimator, named complex single frequency delay estimator (CSFDE), with a serial cancellation procedure, similar to that used by the CLEAN algorithm [35]. However, the CSFDEC algorithm performs target cancellation in the frequency domain, whereas the CLEAN algorithm accomplishes it on the 2D sequence $\{\hat{H}_{m,n}\}$ extracted from the (time domain) received signal. The processing accomplished by the CSFDE algorithm consists in an initialization followed by an iterative procedure. In the initialization, the following quantities are computed: 1) The set of 13 $M_0 \times N_0$ matrices $\{\bar{\mathbf{Y}}_{k_1,k_2} = [\bar{Y}_{k_1,k_2}[l,p]]\}$ (with k_1, $k_2 = 0, 1, 2, 3$, and $(k_1, k_2) \neq (0, 3)$, $(3, 0)$ and $(3, 3)$); here,

$$\bar{\mathbf{Y}}_{k_1,k_2} \triangleq \mathrm{DSFT}\left[\hat{\mathbf{H}}_{k_1,k_2}^{(\mathrm{ZP})}\right] \tag{39}$$

is the order (M_0, N_0) DSFT of the zero padded version

$$\hat{\mathbf{H}}_{k_1,k_2}^{(\mathrm{ZP})} \triangleq \begin{bmatrix} \hat{\mathbf{H}}_{k_1,k_2} & \mathbf{0}_{M,(L_D-1)N} \\ \mathbf{0}_{(L_r-1)M,N} & \mathbf{0}_{(L_r-1)M,(L_D-1)N} \end{bmatrix} \tag{40}$$

of the $M \times N$ matrix $\hat{\mathbf{H}}_{k_1,k_2} \triangleq [\hat{H}_{m,n}^{(k_1,k_2)}]$ and

$$\hat{H}_{m,n}^{(k_1,k_2)} \triangleq m^{k_1} n^{k_2} \hat{H}_{m,n}, \tag{41}$$

with $m = 0, 1, \ldots, M-1$ and $n = 0, 1, \ldots, N-1$ (the oversampling factors L_D and L_r are defined by (22) and (23), respectively).

2) The coarse estimates $\hat{F}_{D,c}^{(0)} = \hat{l}^{(0)}/M_0 - 1/2$ and $\hat{F}_{r,c}^{(0)} = \hat{p}^{(0)}/N_0$ of the normalized Doppler F_D and normalized delay F_r, respectively, that characterize the single target detected by the algorithm; here,

$$\left(\hat{l}^{(0)}, \hat{p}^{(0)}\right) = \arg \max_{\tilde{l} \in \mathcal{S}_{M_0}, \tilde{p} \in \mathcal{S}_{N_0}} \left|\bar{Y}_{0,0}[\tilde{l}, \tilde{p}]\right|^2. \tag{42}$$

3) The initial estimate

$$\hat{A}^{(0)} = \bar{Y}\left(\hat{F}_{D,c}^{(0)}, \hat{F}_{r,c}^{(0)}\right), \tag{43}$$

of the complex amplitude A of the detected target; here,

$$\bar{Y}\left(\tilde{F}_D, \tilde{F}_r\right) \triangleq \frac{1}{MN} \sum_{m=0}^{M-1} \sum_{n=0}^{N-1} \hat{H}_{m,n}\, a_m\left(-\tilde{F}_D\right) a_n\left(\tilde{F}_r\right). \tag{44}$$

4) The coefficients

$$b_\Omega = \hat{\Delta}^3\, \Im\{\hat{A}^* \bar{Y}_{2,3}\}/3 - \hat{\Delta}^2\, \Re\{\hat{A}^* \bar{Y}_{2,2}\} - 2\hat{\Delta}\, \Im\{\hat{A}^* \bar{Y}_{2,1}\} + 2\Re\{\hat{A}^* \bar{Y}_{2,0}\}, \tag{45}$$

$$c_\Omega = \hat{\Delta}^3\, \Re\{\hat{A}^* \bar{Y}_{1,3}\}/3 + \hat{\Delta}^2\, \Im\{\hat{A}^* \bar{Y}_{1,2}\} - 2\hat{\Delta}\, \Re\{\hat{A}^* \bar{Y}_{1,1}\} - 2\Im\{\hat{A}^* \bar{Y}_{1,0}\}, \tag{46}$$

$$b_\Delta = -\hat{\Omega}^3\, \Im\{\hat{A}^* \bar{Y}_{3,2}\}/3 - \hat{\Omega}^2\, \Re\{\hat{A}^* \bar{Y}_{2,2}\} + 2\hat{\Omega}\, \Im\{\hat{A}^* \bar{Y}_{1,2}\} + 2\Re\{\hat{A}^* \bar{Y}_{0,2}\}, \tag{47}$$

and

$$c_\Delta = \hat{\Omega}^3\, \Re\{\hat{A}^* \bar{Y}_{3,1}\}/3 - \hat{\Omega}^2\, \Im\{\hat{A}^* \bar{Y}_{2,1}\} - 2\hat{\Omega}\, \Re\{\hat{A}^* \bar{Y}_{1,1}\} + 2\Im\{\hat{A}^* \bar{Y}_{0,1}\}, \tag{48}$$

where $\bar{Y}_{k_1,k_2} \triangleq \bar{Y}_{k_1,k_2}[\hat{l}^{(0)}, \hat{p}^{(0)}]$ for any k_1 and k_2.

5) The initial estimate $\hat{\Omega}^{(0)}(\hat{\Delta}^{(0)})$ of Ω (Δ) as

$$\hat{X}' = -c_X/b_X, \tag{49}$$

with $X = \Omega$ (with $X = \Delta$).

6) The initial fine estimates

$$\hat{F}_D^{(0)} = \hat{F}_{D,c}^{(0)} + \hat{\Omega}^{(0)}/(2\pi) \tag{50}$$

and

$$\hat{F}_r^{(0)} = \hat{F}_{r,c}^{(0)} + \hat{\Delta}^{(0)}/(2\pi) \tag{51}$$

of F_D and F_r, respectively. This concludes the initialization. The iterative procedure is started by setting the iteration index $i = 1$. The ith iteration is fed by the estimates $\hat{F}_D^{(i-1)}$, $\hat{F}_r^{(i-1)}$ and $\hat{A}^{(i-1)}$ of F_D, F_r and A, respectively, and produces the new estimates $\hat{F}_D^{(i)}$, $\hat{F}_r^{(i)}$ and $\hat{A}^{(i)}$ of the same quantities, with $i = 1, 2, \ldots, N_{\mathrm{it}}$ (where N_{it} is the overall number of iterations selected before starting the algorithm). The procedure adopted for the evaluation of $\hat{F}_D^{(i)}$, $\hat{F}_r^{(i)}$ and $\hat{A}^{(i)}$ consists of the two steps described below.

1) *Estimation of the normalized Doppler and the normalized delay* — The new estimates $\hat{\Omega}^{(i)}$ and $\hat{\Delta}^{(i)}$ of $\tilde{\Omega}$ and $\tilde{\Delta}$, respectively, are computed according to (49). In evaluating the coefficients b_X and c_X (with $X = \Omega$ and Δ) on the

basis of (45)-(48), $\hat{A} = \hat{A}^{(i-1)}$ is assumed; moreover, we set $\bar{Y}_{k_1,k_2} = \bar{Y}_{k_1,k_2}(\hat{F}_D^{(i-1)}, \hat{F}_r^{(i-1)})$ for any k_1 and k_2, where

$$\bar{Y}_{k_1,k_2}\left(\tilde{F}_D, \tilde{F}_r\right) \triangleq \frac{1}{MN} \sum_{m=0}^{M-1} \sum_{n=0}^{N-1} \hat{H}_{m,n}^{(k_1,k_2)} \cdot a_m\left(-\tilde{F}_D\right) a_n\left(\tilde{F}_r\right). \tag{52}$$

An alternative to the use of the last formula for the evaluation of $\bar{Y}_{k_1,k_2}$ is represented by the use of a 2D interpolation method applied to a block of $I_D\, I_r$ elements of the matrix $\bar{\mathbf{Y}}_{k_1,k_2}$ (where I_D and I_r denote the interpolation orders adopted for Doppler and range, respectively); the need of interpolation originates from the fact that, in general, $\hat{F}_D^{(i-1)}$ and $\hat{F}_r^{(i-1)}$ cannot be put in the form (20) and (21) (with a proper choice of the integers l and p), respectively.

Given $\hat{\Omega}^{(i)}$ and $\hat{\Delta}^{(i)}$, the new estimates

$$\hat{F}_D^{(i)} = \hat{F}_D^{(i-1)} + \hat{\Omega}^{(i)}/(2\pi) \tag{53}$$

and

$$\hat{F}_r^{(i)} = \hat{F}_r^{(i-1)} + \hat{\Delta}^{(i)}/(2\pi) \tag{54}$$

are computed.

2) *Estimation of the complex amplitude* — The new estimate $\hat{A}^{(i)}$ of $\hat{A}$ is evaluated by means of (43); in doing so, the couple $(\hat{F}_D^{(i)}, \hat{F}_r^{(i)})$ is used in place of $(\hat{F}_{D,c}^{(0)}, \hat{F}_{r,c}^{(0)})$.

Then, before starting the next iteration, the index i is incremented by one. At the end of the last (i.e., of the $N_{\rm it}$th) iteration, the fine estimates $\hat{F}_D = \hat{F}_D^{(N_{\rm it})}$, $\hat{F}_r = \hat{F}_r^{(N_{\rm it})}$ and $\hat{A} = \hat{A}^{(N_{\rm it})}$ of F_D, F_r and A, respectively, become available and the algorithm stops.

The CSFDE algorithm represents the core of the CSFDEC algorithm, which is used to recursively estimate the multiple tones forming the useful component of the 2D complex sequence $\{\hat{H}_{m,n}\}$, whose (m,n)th element is expressed by (16), with $K \geq 1$ and, in general, *unknown*. The CSFDEC algorithm is initialized by: 1) running the CSFDE algorithm to compute the initial estimates $\hat{F}_{D_0}^{(0)}$, $\hat{F}_{r_0}^{(0)}$ and $\hat{A}_0^{(0)}$ of the parameters F_{D_0}, F_{r_0} and A_0 characterizing the first (i.e., the strongest) target; 2) setting the recursion index i to 1 and $\bar{\mathbf{Y}}_{0,0}^{(0)} = \bar{\mathbf{Y}}_{0,0}$ (see (39) with $k_1 = k_2 = 0$). Then, a recursive procedure is started. The ith recursion of this procedure is fed by the vectors $\hat{\mathbf{F}}_D^{(i-1)} = [\hat{F}_{D_0}^{(i-1)}, \hat{F}_{D_1}^{(i-1)}, \ldots, \hat{F}_{D_{i-1}}^{(i-1)}]^T$, $\hat{\mathbf{F}}_r^{(i-1)} = [\hat{F}_{r_0}^{(i-1)}, \hat{F}_{r_1}^{(i-1)}, \ldots, \hat{F}_{r_{i-1}}^{(i-1)}]^T$ and $\hat{\mathbf{A}}^{(i-1)} = [\hat{A}_0^{(i-1)}, \hat{A}_1^{(i-1)}, \ldots, \hat{A}_{i-1}^{(i-1)}]^T$, collecting the estimates of the normalized Doppler frequency, normalized delay and complex amplitude, respectively, of the i tones detected and estimated in the previous recursions, and generates the new vectors $\hat{\mathbf{F}}_D^{(i)}$, $\hat{\mathbf{F}}_r^{(i)}$ and $\hat{\mathbf{A}}^{(i)}$ after: a) estimating the parameters $\hat{F}_{D_i}^{(i)}$, $\hat{F}_{r_i}^{(i)}$ and $\hat{A}_i^{(i)}$ of the new (i.e., of the ith) tone (if any); b) refining the estimates of the i tones available at the beginning of the considered recursion. The procedure employed for accomplishing all this consists of three steps and can be summarised as follows. In its first step, the *residual spectrum* $\mathbf{Y}_{0,0}^{(i)}$ is computed by subtracting from $\mathbf{Y}_{0,0}^{(i-1)}$ the contribution given by the i estimated 2D tones. If the overall energy $\varepsilon_{0,0}[i] \triangleq \|\mathbf{Y}_{0,0}^{(i)}\|^2$ of the vector $\mathbf{Y}_{0,0}^{(i)}$ satisfies the inequality $\varepsilon_{0,0}[i] < \mathcal{T}_{\rm CSFDEC}$, where $\mathcal{T}_{\rm CSFDEC}$ is a proper threshold, the ith tone has to be considered as the last one; for this reason, the estimate $\hat{K} = i$ of K is generated and the algorithm stops after carrying out the next two steps. In the second step, $N_{\rm it}$ iterations are executed to refine the estimate of the parameters of the new tone detected in the previous step. The processing accomplished in this step follows closely that described in the refinement part (i.e., in the second step) of the CSFDE. Therefore, in each iteration, a new estimate of the complex amplitude and of the two frequency residuals of the ith tone are computed. Finally, in the third step, each tone is re-estimated after cancelling the leakage due to all the other $(i-1)$ tones. This allows to progressively refine the amplitude, normalized Doppler frequency and normalized delay of each tone, thus generating the final estimates of all the detected tones. Note that, in principle, this re-estimation procedure can be repeated multiple (say, $N_{\rm REF}$) times.

Finally, it is worth noting that the refinement procedure of the CSFDEC algorithm does not need, unlike that of the CLEAN algorithm [35], the definition of a search grid for the optimization of a cost function. In fact, the frequency residuals are computed by the CSFDEC on the basis of a closed from expression (see (49)), whose use requires only the knowledge of the spectral coefficients collected in the matrices $\{\bar{\mathbf{Y}}_{k_1,k_2}\}$. It can be shown that the computational cost of the CSFDEC algorithm, when the frequency residuals are evaluated on the basis of (49), is $\mathcal{O}(N_{\rm CSFDEC})$, where (see [33, Sec. III-C, eq. (58)])

$$N_{\rm CSFDEC} = 13\, M_0\, N_0 \log_2(M_0\, N_0) + K^2\, N_{\rm REF}\, N_{\rm it}\; 13\, I_D\, I_r. \tag{55}$$

B. SUBSPACE-BASED METHODS

The use of subspace methods for target range and Doppler estimation has been investigated in [9], [37], [38], and [39]. In particular, algorithms based on the Multiple Signal Classification (MUSIC) technique have been analyzed in [9], [20], [37], and [39], whereas the use of the 2D estimation of signal parameters via rotational invariant technique (ESPRIT) for the estimation of the delay and Doppler of multiple targets has been studied in [38]. Various results illustrated in the above mentioned manuscripts lead to the conclusion that MUSIC-based algorithms can outperform 2D FFT-based methods for joint range-velocity estimation at the price, however, of a significantly larger computational complexity [37]. A lower complexity version of the MUSIC technique, called *auto-paired method*, has been proposed in [39], whereas an iterative method for improving the robustness of the MUSIC algorithm has been developed in [9].

In the following we concentrate on the 2D-MUSIC algorithm only, since it performs similarly as the 2D-ESPRIT at a comparable computational cost [40], [41]. This algorithm is based on the search of $\hat{K}$ local maxima in the 2D-MUSIC spectrum (also known as *pseudo spectrum*),

whose computation requires the identification of the so called *noise subspace*. In practice, the algorithm needs a prior estimate (denoted $\hat{K}$) of K and consists of the following steps:

1) The $(M\,N) \times (M\,N)$ correlation matrix

$$\mathbf{R} \triangleq \frac{1}{MN}\bar{\mathbf{H}}\,\bar{\mathbf{H}}^{H} \tag{56}$$

is evaluated; here, $\bar{\mathbf{H}}$ denotes the (MN)-dimensional vector generated by the ordered concatenation of the columns of the $M \times N$ matrix $\hat{\mathbf{H}} = [\hat{H}_{m,n}]$ (see (16)).

2) The *pseudo-spectrum*

$$P_{\text{MUSIC}}\,[l, p] \triangleq \left\| \mathbf{Q}_{\text{n}}^{H}\,\bar{\mathbf{M}}\,[l, p] \right\|^{-2} \tag{57}$$

is computed for $l = 0, 1, \ldots, M_0 - 1$ and $p = 0, 1, \ldots, N_0 - 1$; here, M_0 and N_0 are integer parameters defining the size of the search space for the normalized Doppler frequency and the normalized delay, respectively, $\bar{\mathbf{M}}[l, p]$ is a $(MN) \times (M_0\,N_0)$ matrix whose (m, n)th element is defined by the product $a_m(F_D[l])\,a_n(-F_r[p])$ (with $F_D[l]$ and $F_r[p]$ expressed by (20) and (21), respectively) and $\mathbf{Q}_{\text{n}}$ is $(MN) \times (MN - \hat{K})$ matrix, whose columns represent the $(MN - \hat{K})$ eigenvectors of $\mathbf{R}$ (56) associated with noise.[8]

3) The estimates of the normalized delay and of the normalized Doppler frequency are evaluated by finding the global maximum of the pseudo-spectrum (57) in the case of a single target or its $\hat{K}$ highest local peaks in the case of multiple targets. Note that, in the last case, all the local maxima of the cost function can be really identified if the spacing between all the targets is greater than the grid step size; this problem can be mitigated by using a finer grid (i.e., a smaller step size) at the price, however, of a larger computational complexity.

The overall 2D-MUSIC complexity is $\mathcal{O}(N_{\text{MUSIC}})$, where

$$N_{\text{MUSIC}} = C_{\text{R}} + C_{\text{e}} + C_{\text{P}}. \tag{58}$$

Here, we have that: a) $C_{\text{R}} = 10(MN)^2 + 2MN - 2$ is the cost due to the computation of the covariance matrix $\mathbf{R}$ (56); b) $C_{\text{e}} \approx (MN)^3$ is the contribution due to computation of the eigenvalues of the matrix $\mathbf{R}$ (56); c) $C_{\text{P}} = M_0\,N_0(8(M\,N)^2 + M\,N)$ is the contribution due to the evaluation of the pseudo-spectrum (see (57)).

C. MAXIMUM LIKELIHOOD-BASED TECHNIQUES

Maximum likelihood-based algorithms are able to achieve an accuracy comparable to that of subspace methods at the price of an increase in computational complexity [41], [42], [43], [44]. Recent research contributions to this field concern: 1) the exploitation of *alternating maximization* approach to mitigate the computational complexity of ML estimation [41]; 2) the derivation of an iterative non-linear kernel least mean square (KLMS) based estimation technique for the estimation of target range [42]; 3) the development of an ML method, based on a kinematic model of detected targets, for estimating target speed [44].

[8]This is true in the absence of fully correlated targets, i.e. when the span of the useful signal subspace is $\hat{K}$-dimensional.

In the following, we first take into consideration the approximate ML methods recently proposed in [41] and show how they can be adapted to our signal model[9] (16); the resulting algorithms, are dubbed *modified Zhang* ML (MZML) and *modified alternating projection* ML (MAP-ML). Both these algorithms are iterative; however, the first one maximizes a 2D cost function, whereas the second one exploits the method of alternating projections to turn a 2D optimization problem into a couple of simpler 1D sub-problems in order to mitigate the overall computational effort. Finally, we take into consideration the modified Wax & Leshem (MWL) algorithm developed in [35] and [36] for joint range and azimuth estimation of multiple targets in FMCW radar systems, and the expectation maximization (EM) algorithm developed in [36] and [41]. In particular, the last algorithm is exploited as follows. It is initialized be means of the 2D-FFT technique. Then, in each of its iterations, it accomplishes leakage compensation in the same way as the MZML algorithm. The resulting algorithm is denoted *Modified Zhang* EM (MZEM) in the following.

1) MODIFIED ZHANG MAXIMUM LIKELIHOOD ALGORITHM

This algorithm operates in an iterative fashion; in each of its iterations, the estimates of the detected targets are refined. It is initialized by: 1) setting the iteration index i to 1; 2) selecting the initial estimate of the normalized Doppler frequency F_{D_k} and that of the normalized delay F_{r_k} as $\hat{F}_{D_k}^{(0)} = F_D[\hat{l}_k^{(0)}]$ and $\hat{F}_{r_k}^{(0)} = F_r[\hat{p}_k^{(0)}]$, respectively (see (20) and (21)), where $(\hat{l}_k^{(0)}, \hat{p}_k^{(0)})$ is computed on the basis of (24) (with $k = 0, 1, \ldots, \hat{K} - 1$, where $\hat{K}$ denotes our prior estimate of K). Then, its iterations are started. The input of the ith iteration (with $i = 1, 2, \ldots, N_{\text{REF}}$, where N_{REF} denotes the overall number of iterations) is represented by the $\hat{K}$-dimensional vectors

$$\hat{\mathbf{F}}_D^{(i-1)} = \left[\hat{F}_{D_0}^{(i-1)}, \hat{F}_{D_1}^{(i-1)}, \ldots, \hat{F}_{D_{\hat{K}-1}}^{(i-1)}\right]^T \tag{59}$$

and

$$\hat{\mathbf{F}}_r^{(i-1)} = \left[\hat{F}_{r_0}^{(i-1)}, \hat{F}_{r_1}^{(i-1)}, \ldots, \hat{F}_{r_{\hat{K}-1}}^{(i-1)}\right]^T, \tag{60}$$

that collect the estimates of the normalized Doppler frequency and the normalized delay, respectively, of the $\hat{K}$ tones estimated in the previous $(i-1)$ iterations, and produces the new estimates $\hat{\mathbf{F}}_D^{(i)}$ and $\hat{\mathbf{F}}_r^{(i)}$. Moreover, in the ith iteration, two distinct steps, that are repeated sequentially for each target (i.e., for $k = 0, 1, \ldots, \hat{K} - 1$), are executed; the description of these steps is provided below for the kth target.

1) *Computation of the cost function* — In this step, the cost function

$$J_k^{(i)}\big(\tilde{F}_{D_k}, \tilde{F}_{r_k}\big) \triangleq \bar{\mathbf{H}}^{H}\,\mathbf{P}_k^{(i)}\big(\tilde{F}_{D_k}, \tilde{F}_{r_k}\big)\bar{\mathbf{H}} \tag{61}$$

[9]Note that, in our model, unlike the one considered in [41], *inter-pulse* and *inter-subcarrier* Doppler effects are neglected.

is evaluated for $(\tilde{F}_{D_k}, \tilde{F}_{r_k}) \in \mathcal{I}_D^{(i)}(M_0) \times \mathcal{I}_r^{(i)}(N_0)$; here, $\mathcal{I}_X^{(i)}(Y)$ denotes the set[10] of Y trial values selected for $\tilde{F}_{X_k}$ (with $X = D$ and r) in the ith iteration, $\bar{\mathbf{H}}$ is the (MN)-dimensional vector resulting from the ordered concatenation of the columns of the $M \times N$ matrix $\hat{\mathbf{H}}_{m,n} = [\hat{H}_{m,n}]$ (see (16)),

$$\mathbf{P}_k^{(i)}(\tilde{F}_{D_k}, \tilde{F}_{r_k}) \triangleq \breve{\mathbf{M}}_k^{(i)} \left((\breve{\mathbf{M}}_k^{(i)})^H \breve{\mathbf{M}}_k^{(i)} \right)^{-1} (\breve{\mathbf{M}}_k^{(i)})^H \tag{62}$$

is the $(MN) \times (MN)$ *orthogonal projection matrix*,

$$\breve{\mathbf{M}}_k^{(i)} \triangleq \Big[\mathbf{M}_0^{(i-1)}, \mathbf{M}_1^{(i-1)}, \ldots, \mathbf{M}_{k-1}^{(i-1)}, \mathbf{M}_{k+1}^{(i-1)}, \ldots, \mathbf{M}_{\hat{K}-1}^{(i-1)}, \dot{\mathbf{M}}_k^{(i)} \Big] \tag{63}$$

is a $(MN) \times \hat{K}$ matrix.[11] The uth element of the last matrix, namely $\mathbf{M}_u^{(i-1)} = \mathbf{M}_u^{(i-1)}(\hat{F}_{D_u}^{(i-1)}, \hat{F}_{r_u}^{(i-1)})$ is an (MN)-dimensional column vector that results from the ordered concatenation of the columns of the $M \times N$ matrix $\hat{\mathbf{M}}_u^{(i-1)}$, whose element (m, n) is expressed by the product $a_m(\hat{F}_{D_u}^{(i-1)})\, a_n(-\hat{F}_{r_u}^{(i-1)})$ for any $u \neq k$ (see (5)), and $\dot{\mathbf{M}}_k^{(i)}$ is an (MN)-dimensional column vector generated by the ordered concatenation of the columns of the $M \times N$ matrix $\tilde{\mathbf{M}}_k^{(i)}$, whose element (m, n) is expressed by the product $a_m(\tilde{F}_{D_k})\, a_n(-\tilde{F}_{r_k})$. It is worth pointing out that: 1) the vector $\mathbf{M}_u^{(i-1)}$ represents the contribution of the uth target (with $u \neq k$), evaluated on the basis of its parameters estimated in the $(i-1)$th iteration, to the vector $\dot{\mathbf{M}}_k^{(i)}$ (computed for the kth target in the ith iteration); 2) evaluating the matrix $\breve{\mathbf{M}}_k^{(i)}$ on the basis of (63) allows to compensate for the spectral *leakage* affecting the projection matrix $\mathbf{P}_k^{(i)}(\cdot, \cdot)$ (62); 3) the sets $\mathcal{I}_D^{(i)}(M_0)$ and $\mathcal{I}_r^{(i)}(N_0)$ are generated by means of the same procedure illustrated for the CLEAN algorithm [35] in Section III-A2 (see (33)-(35), in Table 1).

2) *Target parameter estimation* — In this step, the estimates $\hat{F}_{D_k}^{(i)}$ and $\hat{F}_{r_k}^{(i)}$ of F_{D_k} and F_{r_k} are computed as

$$(\hat{F}_{D_k}^{(i)}, \hat{F}_{r_k}^{(i)}) = \underset{(\tilde{F}_{D_k}, \tilde{F}_{r_k}) \in \mathcal{I}_D^{(i)}(M_0) \times \mathcal{I}_r^{(i)}(N_0)}{\arg\max} \left| J_k^{(i)}(\tilde{F}_{D_k}, \tilde{F}_{r_k}) \right|, \tag{64}$$

Then, the new estimate $\hat{A}_k^{(i)}$ of the complex amplitude A_k is evaluated as

$$\hat{A}_k^{(i)} = \left(\left(\breve{\mathbf{M}}_k^{(i)}(\hat{F}_{D_k}^{(i)}, \hat{F}_{r_k}^{(i)}) \right)^H \breve{\mathbf{M}}_k^{(i)}(\hat{F}_{D_k}^{(i)}, \hat{F}_{r_k}^{(i)}) \right)^{-1} \cdot \left(\breve{\mathbf{M}}_k^{(i)}(\hat{F}_{D_k}^{(i)}, \hat{F}_{r_k}^{(i)}) \right)^H. \tag{65}$$

At the end of the last iteration, the vectors $\hat{\mathbf{F}}_D^{(N_{\text{REF}})}$, $\hat{\mathbf{F}}_r^{(N_{\text{REF}})}$ and $\hat{\mathbf{A}}^{(N_{\text{REF}})}$, collecting the normalized frequencies, the normalized delays and the complex amplitudes of the $\hat{K}$ targets are available.

[10] Once again, the dependence of $\mathcal{I}_X^{(i)}(Y)$ on the target index k is omitted for simplicity. This consideration also applies to the set of trial values employed by the MZML and the MZEM algorithms.

[11] The dependence of the matrices $\breve{\mathbf{M}}_k^{(i)}$, $\tilde{\mathbf{M}}_k^{(i)}$ and of the vector $\dot{\mathbf{M}}_k^{(i)}$ (see below) on the trial variables $\tilde{F}_{D_k}$ and $\tilde{F}_{r_k}$ is not always explicitly shown for simplicity. For the same reason, the dependence of $\hat{\mathbf{M}}_u^{(i-1)}$ (see below) on $\hat{F}_{D_u}^{(i-1)}$ and $\hat{F}_{r_u}^{(i-1)}$ is not indicated.

The overall computational cost of MZML algorithm can be expressed as

$$\mathcal{C}_{\text{MZML}} \triangleq \mathcal{C}_{0,\text{MZML}} + N_{\text{REF}}\, \mathcal{C}_{i,\text{MZML}}, \tag{66}$$

where $\mathcal{C}_{0,\text{MZML}}$ is the cost of its initialization (i.e., the same cost as the 2D-FFT method; see (26)), whereas

$$\mathcal{C}_{i,\text{MZML}} \triangleq \mathcal{C}_P + \mathcal{C}_J + \mathcal{C}_{\text{opt}} \tag{67}$$

represents the cost of a single iteration; here, we have that: 1) $\mathcal{C}_P \approx 8 M_0 N_0 \hat{K}^2 M^2 N^2$ ($\mathcal{C}_J \approx 8 M_0 N_0 \hat{K} M^2 N^2$) is the cost due to the evaluation of the projection matrix $\mathbf{P}_k^{(i)}(\cdot, \cdot)$ (62) (of the function $J_k^{(i)}(\cdot, \cdot)$ (61)) for all the $M_0 N_0$ nodes of the grid and all the $\hat{K}$ targets; 2) $\mathcal{C}_{\text{opt}} = 4 M_0 N_0 \hat{K}$ is the cost due to solving the optimization problem in (64). Based on these results, it can be shown that the computational cost of MZML algorithm is $\mathcal{O}(N_{\text{MZML}})$, where

$$N_{\text{MZML}} = N_{\text{REF}}\, 8\, M_0 N_0 \left(\hat{K}^2 + \hat{K} \right) M^2 N^2. \tag{68}$$

2) MODIFIED ALTERNATING PROJECTION MAXIMUM LIKELIHOOD ALGORITHM

The MAP-ML algorithm is initialized exactly in the same way as the MZML algorithm (see [41]) and employs the cost function $J_k^{(i)}(\tilde{F}_{D_k}, \tilde{F}_{r_k})$ (61) in the estimation of the parameters of the kth target; however, the method of *alternating projection* is exploited for the maximization of that cost function in order to replace the 2D optimization problem (64) with two 1D optimization problems. In practice, in its ith iteration, the frequency estimates $\hat{F}_{D_k}^{(i)}$ and $\hat{F}_{r_k}^{(i)}$ appearing in the *left-hand side* of (64) are evaluated as

$$\hat{F}_{r_k}^{(i)} = \arg \max_{\tilde{F}_{r_k} \in \mathcal{I}_r^{(i)}(N_0)} \left| J_k^{(i)}(\hat{F}_{D_k}^{(i-1)}, \tilde{F}_{r_k}) \right| \tag{69}$$

and

$$\hat{F}_{D_k}^{(i)} = \arg \max_{\tilde{F}_{D_k} \in \mathcal{I}_D^{(i)}(M_0)} \left| J_k^{(i)}(\tilde{F}_{D_k}, \hat{F}_{r_k}^{(i)}) \right|, \tag{70}$$

respectively (the sets $\mathcal{I}_r^{(i)}(N_0)$ and $\mathcal{I}_D^{(i)}(M_0)$ have been already defined for the MZML algorithm). It is important to note that: 1) the evaluation of $J_k^{(i)}(\hat{F}_{D_k}^{(i-1)}, \tilde{F}_{r_k})$ and $J_k^{(i)}(\tilde{F}_{D_k}, \hat{F}_{r_k}^{(i)})$ in the RHSs (69) and (70) requires computing the matrices $\breve{\mathbf{M}}_k^{(i)}(\hat{F}_{D_k}^{(i-1)}, \tilde{F}_{r_k})$ and $\breve{\mathbf{M}}_k^{(i)}(\tilde{F}_{D_k}, \hat{F}_{r_k}^{(i)})$ (see (63)), respectively; 2) in the first iteration (i.e., for $i = 1$), $\hat{F}_{D_k}^{(0)}$ is computed according to (20), with $l = \hat{l}_k^{(0)}$, where $\hat{l}_k^{(0)}$ results from solving (24) (the value of p, $\hat{p}_k^{(0)}$, associated with $\hat{l}_k^{(0)}$ is discarded); 3) the estimate of the complex amplitude $\hat{A}_k^{(i)}$ is computed on the basis of (65).

The overall computational cost $\mathcal{C}_{\text{MAP-ML}}$ of the MAP-ML algorithm can be expressed as

$$\mathcal{C}_{\text{MAP-ML}} = \mathcal{C}_{0,\text{MAP-ML}} + N_{\text{REF}}\, \mathcal{C}_{i,\text{MAP-ML}}, \tag{71}$$

where $\mathcal{C}_{0,\text{MAP-ML}}$ is the contribution due to its initialization (equal to $\mathcal{C}_{0,\text{MZML}}$; see (66)), whereas

$$\mathcal{C}_{i,\text{MAP-ML}} = \mathcal{C}_{P_r} + \mathcal{C}_{P_D} + \mathcal{C}_{J_r} + \mathcal{C}_{J_D} + \mathcal{C}_r + \mathcal{C}_D \tag{72}$$

is the contribution due to each of its iterations. Moreover, in the last formula, we have that: 1) $\mathcal{C}_{P_r} \approx 8N_0\hat{K}^2M^2N^2$ and $\mathcal{C}_{P_D} \approx 8M_0\hat{K}^2M^2N^2$ are the costs due to the evaluation of the projection matrix $\mathbf{P}_k^{(i)}(\cdot,\cdot)$ (62) in the first and second 1D optimization, respectively; 2) $\mathcal{C}_{J_r} \approx 8N_0\hat{K}M^2N^2$ and $\mathcal{C}_{J_D} \approx 8M_0\hat{K}M^2N^2$ are the costs due to the evaluation of the function $J_k^{(i)}(\cdot,\cdot)$ (61) in the first and second 1D optimization, respectively; 3) $\mathcal{C}_r = 4N_0$ and $\mathcal{C}_D = 4M_0$ are the costs required by solving the 1D maximization in (69) and (70), respectively.

Based on (71)-(72), it can be shown that the computational cost of MAP-ML algorithm is $\mathcal{O}(N_{\text{MAP-ML}})$, where

$$N_{\text{MAP-ML}} = N_{\text{REF}}\, 8(M_0+N_0)\,(\hat{K}^2+\hat{K})\,M^2N^2. \tag{73}$$

3) MWL ALGORITHM

Similarly as the CLEAN algorithm [35], the MWL algorithm operates in an iterative fashion and, in each of its iterations, estimates the parameters of a new target, and performs cancellation and leakage compensation in the time domain. However, unlike the CLEAN algorithm, the MWL algorithm requires solving 1D optimization problems only. Moreover, it can achieve similar and even better accuracy than the CLEAN algorithm with a smaller computational effort [36].

The MWL algorithm is initialized by setting the iteration index k to 0 and $\hat{H}_{m,n}[0] = \hat{H}_{m,n}$ (see (16)), with $m = 0, 1, \ldots, M-1$ and $n = 0, 1, \ldots, N-1$. Then, its iterations are started; the processing accomplished in the kth iteration evolves through the four steps described below.

1) *Coarse estimation of the Doppler of a new target* — In this step, the *coarse estimate* $\breve{F}_{D_k}$ of the Doppler frequency F_{D_k} of a new (namely, of the kth) target is computed by solving the 1D optimization problem

$$\breve{l}_k \triangleq \arg\max_{\tilde{l}\in\mathcal{S}_{M_0}} \mathbf{a}^H\big(F_D[\tilde{l}]\big)\mathbf{R}\,[k]\;\mathbf{a}\big(F_D[\tilde{l}]\big), \tag{74}$$

where $F_D[\tilde{l}]$ is defined by (20), $\mathbf{a}(F_D[\tilde{l}])$ is an M-dimensional column vector whose mth element (with $m = 0, 1, \ldots, M-1$) is $a_m(F_D[\tilde{l}])$ (see (5)), $\mathbf{R}[k] = [R_{m,m'}[k]]$ is an $M \times M$ autocorrelation matrix such that

$$R_{m,m'}\,[k] \triangleq \frac{1}{N}\sum_{n=0}^{N-1} \hat{H}_{m,n}\,[k]\left(\hat{H}_{m',n}\,[k]\right)^H, \tag{75}$$

where $\hat{H}_{m,n}[k]$ is evaluated on the basis of (29) if $k > 0$, with $m = 0, 1, \ldots, M-1$ and $m' = 0, 1, \ldots, M-1$. Given $\breve{l}_k$ (74), the coarse estimate of F_{D_k} is computed as $\breve{F}_{D_k} = F_D[\breve{l}_k]$ (see (20)).

2) *Estimation of target delay* — In this step, an estimate $\hat{F}_{r_k}$ of the normalized delay F_{r_k} characterizing the kth target is evaluated by solving another 1D optimization problem. This requires:

a) Computing the N-dimensional column vector

$$\hat{\mathbf{v}}_k \triangleq \big[\hat{v}_k[0], \hat{v}_k[1], \ldots, \hat{v}_k[N-1]\big]^T, \tag{76}$$

where

$$\hat{v}_k[n] \triangleq \left[\mathbf{a}^H\big(\breve{F}_{D_k}\big)\,\mathbf{a}\big(\breve{F}_{D_k}\big)\right]^T \mathbf{a}^H\big(\breve{F}_{D_k}\big)\,\mathbf{H}_n\,[k]\,, \tag{77}$$

with $n = 0, 1, \ldots, N-1$, and $\mathbf{H}_n[k] \triangleq [\hat{H}_{0,n}[k], \hat{H}_{1,n}[k], \ldots, \hat{H}_{M-1,n}[k]]^T$ is an M-dimensional vector.

b) Evaluating

$$\hat{p}_k = \arg\max_{\tilde{p}\in\mathcal{S}_{N_0}} \left\|\mathbf{a}^H\left(-F_r\left[\tilde{p}\right]\right)\,\hat{\mathbf{v}}_k\right\|^2, \tag{78}$$

where $F_r[\tilde{p}]$ is defined by (21), and $\mathbf{a}(-F_r[\tilde{p}])$ is an N-dimensional column vector whose n-element (with $n = 0, 1, \ldots, N-1$) is $a_n(-F_r[\tilde{p}])$ (see (5)). Given $\hat{p}_k$ (78), the final estimate $\hat{F}_{r_k}$ of the target delay is evaluated according to (21) with $p = \hat{p}_k$.

3) *Fine estimation of target Doppler* — In this step, the *fine estimate* $\hat{F}_{D_k}$ of the normalized Doppler F_{D_k} characterizing the kth target is evaluated by solving the last 1D optimization problem and, in particular, as $\hat{F}_{D_k} = F_D[\hat{l}_k]$ (see (20)), where

$$\hat{l}_k \triangleq \arg\max_{\tilde{l}\in\mathcal{S}_{M_0}} \left|\mathbf{a}^H\big(F_D[\tilde{l}]\big)\hat{\mathbf{B}}\big(\hat{F}_{r_k}\big)\right|^2, \tag{79}$$

$\hat{\mathbf{B}}(\hat{F}_{r_k})$ is an M-dimensional row vector, whose mth element is defined as

$$\hat{B}_m\big(\hat{F}_{r_k}\big) \triangleq \left[\sum_{n=0}^{N-1} \hat{H}_{m,n}\,a_n^*\big(-\hat{F}_{r_k}\big)\right]\hat{C}^{-1}\big(\hat{F}_{r_k}\big), \tag{80}$$

and

$$\hat{C}\big(\hat{F}_{r_k}\big) \triangleq \sum_{n=0}^{N-1} a_n\big(-\hat{F}_{r_k}\big)a_n^*\big(-\hat{F}_{r_k}\big). \tag{81}$$

4) *Estimation of target complex amplitude* — In this step, the estimate

$$\hat{A}_k = \left\|\mathbf{a}\big(\hat{F}_{D_k}\big)\right\|^{-2} \mathbf{a}^H\big(\hat{F}_{D_k}\big)\,\hat{\mathbf{B}}\big(\hat{F}_{r_k}\big), \tag{82}$$

of the complex amplitude A_k is evaluated.

Similarly as the CLEAN algorithm [35], at the end of the last step a false target is detected if $|\hat{A}_k| < \mathcal{T}_{\text{MWL}}$, where $\mathcal{T}_{\text{MWL}}$ denotes a proper (positive) threshold. When this occurs, the execution is stopped; otherwise, a new iteration is started going back to step 1).

An iterative procedure can be employed to refine the target estimates generated by the MWL algorithm. Similarly as the CLEAN algorithm, this procedure is based on: 1) estimating again the parameters of each target after removing the spectral contribution of the other $(\hat{K}-1)$ targets, i.e. their *leakage*; 2) shrinking the search grid as iterations evolve (see (33)-(35), in Table 1). In the ith iteration of the refinement (with $i = 1, 2, \ldots, N_{\text{REF}}$), the finer estimates $\{(\hat{F}_{D_k}^{(i)}, \hat{F}_{r_k}^{(i)}, \hat{A}_k^{(i)}); k = 0, 1, \ldots, \hat{K}-1\}$ of the parameters of the $\hat{K}$ targets detected by the MWL algorithm are computed as follows. First, we compute the coarse estimate

$$\breve{F}_{D_k}^{(i)} \triangleq \arg\max_{\tilde{F}_{D_k}\in\mathcal{I}_D^{(i)}\left(\tilde{M}_0\right)} \mathbf{a}^H\big(\tilde{F}_{D_k}\big)\mathbf{R}^{(i)}\,[k]\;\mathbf{a}\big(\tilde{F}_{D_k}\big) \tag{83}$$

of the normalized Doppler frequency for the kth target; here, $\mathcal{I}_D^{(i)}(\tilde{M}_0)$ denotes the set of $\tilde{M}_0$ trial values selected for $\tilde{F}_{D_k}$ in the ith iteration and $\mathbf{R}^{(i)}[k]$ is an $M \times M$ matrix whose element (m, m') is still defined by (75), where, however, $\hat{H}_{m,n}[k]$ is replaced by

$$\check{H}_{m,n}^{(i)}[k] = \hat{H}_{m,n}[0] - \sum_{j=0, j\neq k}^{\hat{K}-1} \hat{A}_j^{(i-1)} \cdot a_m\left(\hat{F}_{D_j}^{(i-1)}\right) a_n\left(-\hat{F}_{r_j}^{(i-1)}\right). \quad (84)$$

Then, we compute

$$\hat{F}_{r_k}^{(i)} = \arg \max_{\tilde{F}_{r_k} \in \mathcal{I}_r^{(i)}\left(\tilde{N}_0\right)} \left\| \mathbf{a}^H\left(-\tilde{F}_{r_k}\right) \hat{\mathbf{v}}_k^{(i)} \right\|^2, \quad (85)$$

where $\mathcal{I}_r^{(i)}(\tilde{N}_0)$ denotes the set of $\tilde{N}_0$ trial values selected for $\tilde{F}_{r_k}$ in the ith iteration, $\mathbf{a}(-\tilde{F}_{r_k})$ is an N-dimensional column vector whose nth element is $a_n(-\tilde{F}_{r_k})$ (see (5)), $\hat{\mathbf{v}}_k^{(i)}$ plays the same role as $\hat{\mathbf{v}}_k$ in (78), but its nth element is defined as (see (77))

$$\hat{v}_k^{(i)}[n] \triangleq \left[\mathbf{a}^H\left(\check{F}_{D_k}^{(i)}\right) \mathbf{a}\left(\check{F}_{D_k}^{(i)}\right)\right]^T \mathbf{a}^H\left(\check{F}_{D_k}^{(i)}\right) \mathbf{H}_n^{(i)}[k], \quad (86)$$

where $\mathbf{H}_n^{(i)}[k] \triangleq [\hat{H}_{0,n}^{(i)}[k], \hat{H}_{1,n}^{(i)}[k], \ldots, \hat{H}_{M-1,n}^{(i)}[k]]^T$. Finally, the new estimate

$$\hat{F}_{D_k}^{(i)} \triangleq \arg \max_{\tilde{F}_{D_k} \in \mathcal{I}_{\tilde{M}_0}^{(i)}} \left| \mathbf{a}^H\left(\tilde{F}_{D_k}\right) \hat{\mathbf{B}}\left(\hat{F}_{r_k}^{(i)}\right) \right|^2 \quad (87)$$

of F_{D_k} is evaluated; here, $\hat{\mathbf{B}}(\hat{F}_{r_k}^{(i)})$ is a M-dimensional row vector, whose mth element (with $m = 0, 1, \ldots, M-1$) is still defined by (80) with $\hat{F}_{r_k}^{(i)}$ in place of $\hat{F}_{r_k}$. This concludes the ith iteration.

The estimates $\{(\hat{F}_{D_k}^{(N_{\mathrm{REF}})}, \hat{F}_{r_k}^{(N_{\mathrm{REF}})}, \hat{A}_k^{(N_{\mathrm{REF}})}); k = 0, 1, \ldots, \hat{K}-1\}$ available at the end of the last (i.e., of the N_{REF}th) iteration represent the output of the refinement algorithm.

It can be shown that the computational cost of the MWL algorithm is $\mathcal{O}(N_{\mathrm{MW}})$, where (see [36, Sec. III-E, eq.(44)])

$$N_{\mathrm{MW}} = \bar{N}_{\mathrm{MW}}(M_0, N_0) + K N_{\mathrm{REF}} \bar{N}_{\mathrm{MW}}(\tilde{M}_0, \tilde{N}_0) \quad (88)$$

and

$$\bar{N}_{\mathrm{MW}}(M_0, N_0) = M^2 (6N + 8M_0) + 30MN + 8N_0 N + 30M_0 M \quad (89)$$

represents the cost due to a single iteration of the algorithm; note that the parameters (M_0, N_0) and $(\tilde{M}_0, \tilde{N}_0)$ define the grid size for the initialization and for the refinement step, respectively.

4) EM-BASED ALGORITHM

The EM algorithm [45] can be employed jointly with each of the algorithms described above to *refine* its estimates of target parameters [36], [41]. For this reason, we can assume that, in general, the EM algorithm is fed by the $\hat{K}$-dimensional vectors $\hat{\mathbf{F}}_D = [\hat{F}_{D_0}, \hat{F}_{D_1}, \ldots, \hat{F}_{D_{\hat{K}-1}}]$, $\hat{\mathbf{F}}_r = [\hat{F}_{r_0}, \hat{F}_{r_1}, \ldots, \hat{F}_{r_{\hat{K}-1}}]$ and $\hat{\mathbf{A}} = [\hat{A}_0, \hat{A}_1, \ldots, \hat{A}_{\hat{K}-1}]$, collecting the *initial estimates* of the normalized Doppler, normalized delay and the complex amplitude of the $\hat{K}$ detected targets.

The EM algorithm operates in an iterative fashion; in each of its iterations, it executes an *expectation step* (E-step) followed by a *maximization step* (M-step). In our description of such steps, we focus on the ith iteration (with $i = 1, \ldots, N_{\mathrm{REF}}$, where N_{REF} denotes the overall number of iterations) and consider the kth target (with $k = 0, 1, \ldots, \hat{K}-1$). At the beginning of this iteration, the estimates $(\hat{F}_{D_k}^{(i-1)}, \hat{F}_{r_k}^{(i-1)}, \hat{A}_k^{(i-1)})$ are available for the normalized Doppler, the normalized delay and the complex amplitude, respectively, of the considered target (if $i = 1$, $(\hat{F}_{D_k}^{(0)}, \hat{F}_{r_k}^{(0)}, \hat{A}_k^{(0)}) = (\hat{F}_{D_k}, \hat{F}_{r_k}, \hat{A}_k)$). The two steps accomplished within the considered iteration are described below.

1) *E step* — In this step, the cost function

$$J_{\mathrm{EM}_k}^{(i)}\left(\tilde{F}_{D_k}, \tilde{F}_{r_k}\right) = \frac{1}{MN} \left\| \left(\check{\mathbf{M}}_k^{(i)}\left(\tilde{F}_{D_k}, \tilde{F}_{r_k}\right)\right)^H \hat{\mathbf{H}}_k^{(i)} \right\|^2, \quad (90)$$

where $(\tilde{F}_{D_k}, \tilde{F}_{r_k}) \in \mathcal{I}_D^{(i)}(M_0) \times \mathcal{I}_r^{(i)}(N_0)$; here, $\mathcal{I}_X^{(i)}(Y)$ denotes the set of Y trial values selected for $\tilde{F}_{X_k}$ (with $X = D$ and r) in the ith iteration. Moreover, the $(MN \times \hat{K})$ matrix $\check{\mathbf{M}}_k^{(i)}(\tilde{F}_{D_k}, \tilde{F}_{r_k})$ is defined by (63),

$$\hat{\mathbf{H}}_k^{(i)} = \hat{\mathbf{H}}_k^{(i-1)} + \beta_k^{(i)} \left[\bar{\mathbf{H}} - \sum_{k'=0}^{\hat{K}-1} \hat{\mathbf{H}}_{k'}^{(i-1)} \right] \quad (91)$$

is the reconstructed (MN)-dimensional vector of channel gains evaluated for the kth target in the ith iteration, $\bar{\mathbf{H}}$ is the (MN)-dimensional vector resulting from the ordered concatenation of the columns of the channel measurement matrix $\hat{\mathbf{H}}_{m,n} \triangleq [\hat{H}_{m,n}]$ (16), $\hat{\mathbf{H}}_k^{(i-1)} \triangleq \hat{A}_k^{(i-1)} \mathbf{M}_k^{(i-1)}$, where $\mathbf{M}_k^{(i-1)}$ is the (MN)-dimensional vector defined after (63) (with $u = k$). Moreover, for any i, the $\hat{K}$ parameters $\{\beta_k^{(i)}; k = 0, 1, \ldots, \hat{K}-1\}$ are the so called *mixing coefficients* and satisfy the inequalities $0 \leqslant \beta_k^{(i)} \leqslant 1$ for any k (e.g., see [36, Sec. III-D]).

2) *M step* — The new (and, hopefully, finer) estimates $\hat{F}_{D_k}^{(i)}$ and $\hat{F}_{r_k}^{(i)}$ of F_{D_k} and F_{r_k}, respectively, are computed as

$$\left(\hat{F}_{D_k}^{(i)}, \hat{F}_{r_k}^{(i)}\right) = \arg \max_{(\tilde{F}_{D_k}, \tilde{F}_{r_k}) \in \mathcal{I}_D^{(i)}(M_0) \times \mathcal{I}_r^{(i)}(N_0)} J_{\mathrm{EM}_k}^{(i)}\left(\tilde{F}_{D_k}, \tilde{F}_{r_k}\right). \quad (92)$$

In the equation above, the term $J_{\mathrm{EM}_k}^{(i)}(\cdot, \cdot)$ evaluated through (90) represents the cost function computed over a specific rectangular grid, defined by the trial values $(\tilde{F}_{D_k}, \tilde{F}_{r_k})$, whose center depends on both $\hat{F}_{D_k}^{(i-1)}$ and $\hat{F}_{r_k}^{(i-1)}$, and whose step sizes gets smaller as i increases. The grid employed in this case is generated according to the same criteria illustrated for the refinement procedure developed for the CLEAN algorithm (see (33)-(35), in Table 1 and the comments related to them).

TABLE 2. Computational complexity order of various estimation algorithms.

Algorithm	2D-FFT method	MWL	2D-MUSIC
$\mathcal{O}(\cdot)$	$M_0\,N_0\log_2(M_0\,N_0)+K(M_0\,N_0)$	$\bar{N}_{\rm MW}(M_0,N_0)+KN_{\rm REF}\,\bar{N}_{\rm MW}(\tilde{M}_0,\tilde{N}_0)$	$(M\,N+M_0\,N_0)(M\,N)^2$
Algorithm	CSFDEC	CLEAN	MZML
$\mathcal{O}(\cdot)$	$13\,M_0\,N_0\log_2(M_0\,N_0)+K^2\,N_{\rm REF}\,N_{\rm it}\;13\,I_D\,I_r$	$\bar{N}_{\rm CL}(M_0,N_0)+N_{\rm REF}\,\bar{N}_{\rm CL}(\tilde{M}_0,\tilde{N}_0)$	$N_{\rm REF}\,8M_0\,N_0(K^2+K)M^2N^2$
Algorithm	MAP-ML	EM	
$\mathcal{O}(\cdot)$	$N_{\rm REF}\,8\,(M_0+N_0)\,(K^2+K)\,M^2N^2$	$N_{\rm REF}[K(14M\,N\,M_0\,N_0)+2K^2M\,N]$	

Finally, the complex amplitude $\hat{A}_k^{(i)}$ is evaluated as (e.g., see [41, Sec IV, eq. (48)]):

$$\hat{A}_k^{(i)}=\frac{1}{MN}\left(\dot{\mathbf{M}}_k^{(i)}\big(\hat{F}_{D_k}^{(i)},\hat{F}_{r_k}^{(i)}\big)\right)^T\hat{\mathbf{H}}_k^{(i)},\tag{93}$$

where $\dot{\mathbf{M}}_k^{(i)}(\cdot,\cdot)$ is defined right after (63). This concludes the M step.

At the end of the last iteration (i.e., for $i=N_{\rm REF}$), the final estimates $(\hat{F}_{D_k}^{(N_{\rm REF})},\hat{F}_{r_k}^{(N_{\rm REF})},\hat{A}_k^{(N_{\rm REF})})$ are available, with $k=0,1,\ldots\hat{K}-1$.

The overall computational cost of a single iteration of the EM algorithm in the presence of $\hat{K}$ targets can be expressed in a similar way as [36, Appendix C], i.e. as

$$N_{\rm EM}=\hat{K}\left(\mathcal{C}_H+\mathcal{C}_{\check{M}}+\mathcal{C}_J+\mathcal{C}_{\rm opt}+\mathcal{C}_A\right),\tag{94}$$

where: 1) $\mathcal{C}_H=2(\hat{K}+2)\,M\,N$ is the contribution due to the computation of (MN)-dimensional vectors $\{\hat{\mathbf{H}}_k^{(i)}\}$ (see (91)); 2) $\mathcal{C}_{\check{M}}=6MNM_0N_0$ is the contribution due to the evaluation of the matrix $\check{\mathbf{M}}_k^{(i)}(\cdot,\cdot)$ appearing in (90); 3) $\mathcal{C}_J=8MNM_0N_0$ is the cost due to the computation of $J_{{\rm EM}_k}^{(i)}(\cdot,\cdot)$ (90), whereas $\mathcal{C}_{\rm opt}=4M_0N_0$ is the cost of its optimization; 4) $\mathcal{C}_A=8MN$ is the cost due to the computation of $\hat{A}_k^{(i)}$ on the basis of (93). In our work, as already mentioned in Subsection III-C, the EM algorithm has been employed to refine the estimates generated by the 2D-FFT algorithm. The overall computational complexity of the resulting algorithm, called MZEM, is $\mathcal{O}(N_{\rm MZEM})$, where $N_{\rm MZEM}=N_{\rm 2D-FFT}+N_{\rm EM}$ (see (26) and (94)).

The computational complexity orders of the estimation algorithms described above and considered in our simulations are listed in Table 2.

IV. NUMERICAL RESULTS

The estimation algorithms described in the previous section have been compared, in terms of accuracy and computational effort, in four distinct scenarios for different values of the *signal-to-noise ratio*

$$\text{SNR}\triangleq\sum_{k=1}^{K}|A_k|^2/\sigma_W^2,\tag{95}$$

where σ_W^2 represents the variance of each element of the complex noise sequence $\{\bar{W}_m(n)\}$ (see (17)). The *first scenario* (**S1**) is characterized by a single target (i.e., by $K=1$), whose range and velocity are uniformly distributed in the intervals [0, 10] m and [0, 2.78] m/s, respectively; the complex amplitude A_0 of its echo, instead, is set to one. The *second scenario* (**S2**) is characterized by four targets (i.e., by $K=4$). The range and velocity of the kth target (with $k=0,1,\ldots,K-1$) are evaluated as

$$R_k=R_0+k\,\bar{R}\,R_{\rm bin}\tag{96}$$

and

$$v_k=v_0+k\,\bar{v}\,v_{\rm bin},\tag{97}$$

respectively, and its amplitude A_k is set to 1 for any k; here, R_0 and v_0 are uniformly distributed in the interval [0, 10] m and [0, 2.78] m/s, respectively. Moreover, $\bar{R}=1.65$ and $\bar{v}=1.65$ represent the spacing of adjacent bins for normalized range and normalized velocity, whereas $R_{\rm bin}\triangleq c/(2\,N\,\Delta_f)$ and $v_{\rm bin}\triangleq c/(2\,M\,f_c\,T_s)$ denote the size of range and velocity bins that characterizes FFT processing in the absence of oversampling, respectively. In both **S1** and **S2**, the accuracy of eight different algorithms (namely, the 2D-FFT, CSFDEC, 2D-MUSIC, CLEAN, MWL, MZML, MAP-ML and MZEM algorithms) has been assessed in terms of *root mean*

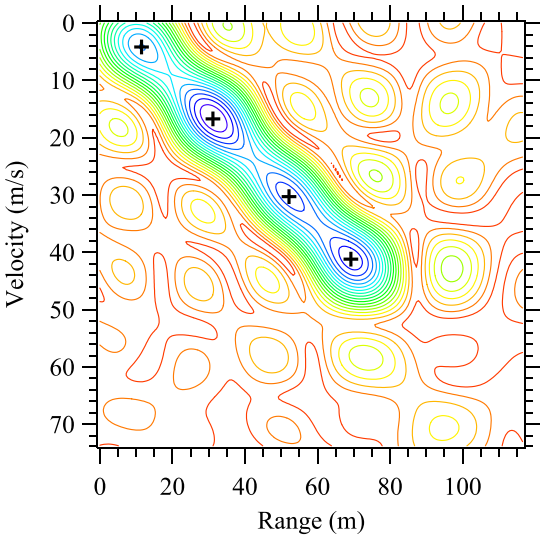

FIGURE 1. The targets are indicated by a cross. *Range-Doppler map* referring to the fourth scenario considered in our simulations.

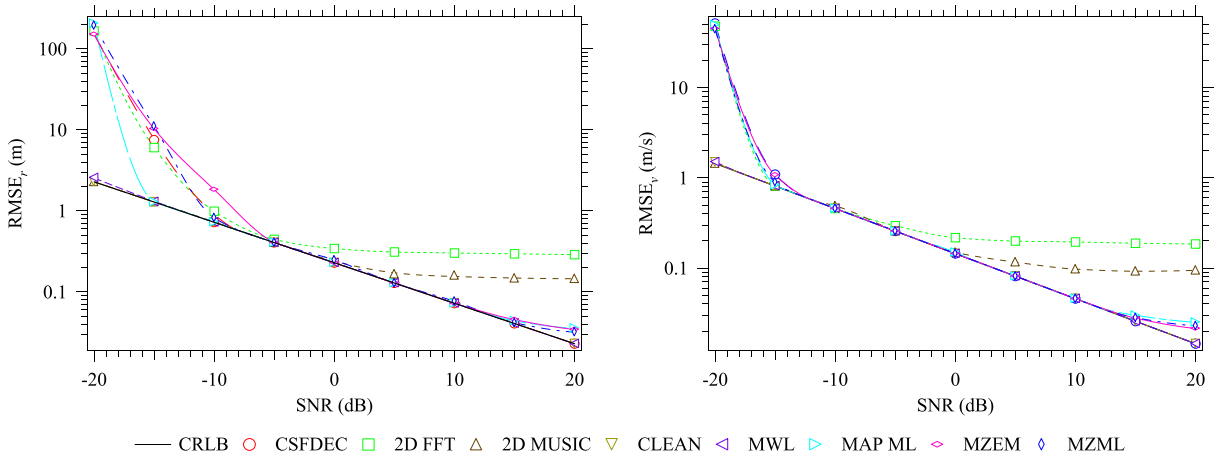

FIGURE 2. Root mean square error performance achieved in range and velocity estimation (first scenario). The 2D-FFT, CSFDEC, CLEAN, MWL, 2D-MUSIC, MZML, MAP-ML and MZEM algorithms are considered.

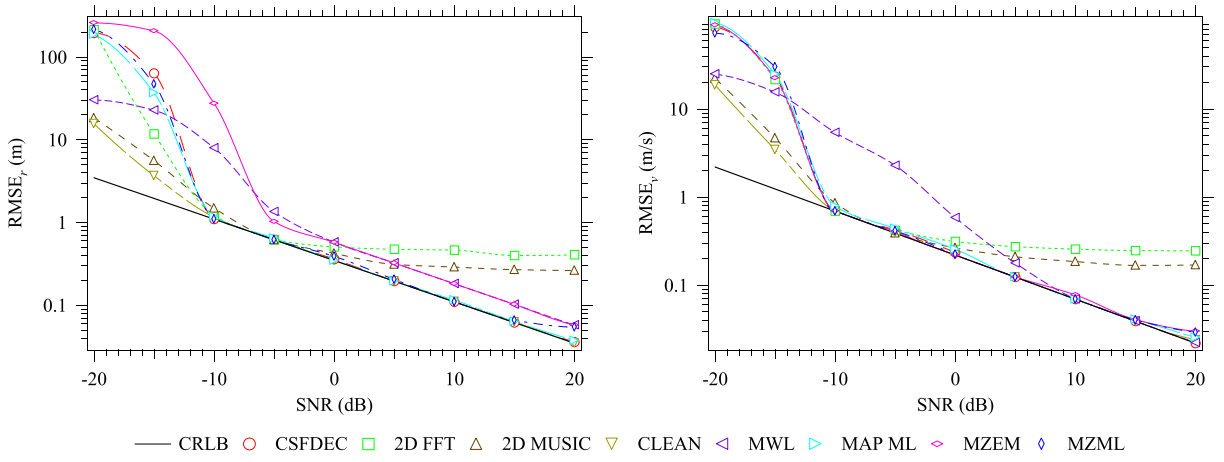

FIGURE 3. Root mean square error performance achieved in range and velocity estimation (second scenario). The 2D-FFT, CSFDEC, CLEAN, MWL, 2D-MUSIC, MZML, MAP-ML and MZEM algorithms are considered.

square error

$$\mathrm{RMSE}_X \triangleq \frac{1}{N_{\mathrm{mc}}} \sum_{t=0}^{N_{\mathrm{mc}}-1} \sqrt{\frac{1}{K} \sum_{k=0}^{K-1} (\hat{X}_k[t] - X_k)^2}, \qquad (98)$$

where $\hat{X}_k[t]$ denotes the estimate of the parameter X_k evaluated for the kth target in the tth Monte Carlo run, N_{mc} is the overall number of runs and $X = r$ ($X = v$) if target range (target velocity) is considered. Moreover, the following choices have been made: 1) in the evaluation of the RMSE$_r$, the vector collecting target ranges and the one collecting their estimates have been organized according to an ascending order (from minimum to maximum range); 2) in the evaluation of the RMSE$_v$, the vector collecting target velocities and the one collecting their estimates are sorted in the same way as the vectors referring to target ranges; 3) an SNR belonging to the interval $[-20, 20]$ dB has been considered; 4) the number of targets (K) has been always assumed to be known (so that events of missed detection are avoided). Note that the knowledge of K does not prevent all the algorithms from identifying false targets; in our work, unwanted detections contribute to the evaluation of the RMSE.

In the *third scenario* (**S3**), the range and velocity of the targets are computed according to the same strategy adopted in **S2**, but the SNR is fixed to 0 dB and the value of K ranges from 1 to 10. In this case, we focus on the *computational effort* required by all the algorithms considered in **S1** and **S2** and, in particular, we assess both their computation time (CT) and the overall number of FLOPs they require.[12]

The *fourth scenario* (**S4**) is characterized by the same number of targets as **S2** (i.e., $K = 4$) and by an SNR equal to 0 dB. Moreover, target ranges and speeds are computed according to (96) and (97), but smaller bin spacings (more precisely, $\bar{R} = 1$ and $\bar{v} = 1$) are assumed. For this reason, in this scenario, spectral leakage may substantially affect target estimation; this can be easily inferred from Fig. 1, where

[12] All the algorithms have been executed on a desktop computer equipped with an i7 processor.

TABLE 3. Main parameters of the search grid selected for the 2D-MUSIC algorithm (range is expressed in m, velocity in m/s).

2D-MUSIC	$[R_{\min}, R_{\max}, N_0]$	$[v_{\min}, v_{\max}, M_0]$
S1	[0, 12, 21]	[0, 3.45, 31]
S2	[0, 120, 201]	[0, 23, 201]
S3	[0, 300, 201]	[0, 57.5, 501]

TABLE 4. Main parameters of the initial search grid selected for the CLEAN and MWL algorithms (range is expressed in m, velocity in m/s).

CLEAN & MWL	$[R_{\min}, R_{\max}, N_0]$	$[v_{\min}, v_{\max}, M_0]$
S1	[0, 12, 21]	[0, 3.45, 31]
S2	[0, 120, 201]	[0, 23, 201]
S3	[0, 300, 501]	[0, 57.5, 501]
S4	[0, 72, 121]	[0, 13.8, 121]

the range-Doppler map (or *ambiguity function*) is shown for the considered case. In our analysis of **S4**, we assess the *convergence speed* of six iterative algorithms (namely, the CSFDEC, CLEAN, MWL, MZML, MAP-ML and MZEM algorithms) and, in particular, we analyze how their accuracy changes as the overall number of their iterations[13] ranges from 1 to 5.

Our interest in the four scenarios defined above can motivated as follows. The numerical results obtained in the first two scenarios show how the considered algorithms perform in the presence of a single tone and of multiple (but *adequately spaced*[14]) tones, respectively, whereas those obtained in the third scenario allow us to assess the trend of their computational requirements when the overall number of targets increases. Finally, the fourth scenario sheds some light on the trade-off between estimation accuracy and computational effort of the considered iterative algorithms in the presence of *closely spaced* targets.

In our simulations, the following choices have been made. First of all, prior knowledge about K has been assumed and, unless differently stated, the following values have been selected for the parameters of the OFDM modulation[15]: 1) overall number of subcarriers $N = 32$; 2) overall number of OFDM symbols/frame $M = 32$; 3) subcarrier spacing $\Delta_f = 250$ kHz; 4) cyclic prefix duration $T_G = 0.25\ T = 1\mu$s (consequently, the OFDM symbol duration is $T_s = 1/\Delta_f + T_G = 5\ \mu$s); 5) carrier frequency $f_c = 79$ GHz. These values entail that $R_{\text{bin}} = 18.7$ m and $v_{\text{bin}} = 12$ m/s.

Secondly, the following values have been selected for the parameters of the considered algorithms: 1) the oversampling factor $L_D = 16$ and $L_r = 16$ have been chosen for Doppler and range estimation, respectively, in both the 2D-FFT and CSFDEC algorithms (so that $M_0 = ML_D = 512$ and $N_0 = NL_r = 512$; see (22) and (23), respectively); 2) the 2D-FFT method has been used to compute the initial estimates

[13] In the case of the CSFDEC algorithm, each iteration corresponds to the execution of the re-estimation procedure described in Subsection III-A3.

[14] This means that the spectral leakage affecting each tone and originating from all the other tones is limited; therefore, the frequency estimation error due to this phenomenon is negligible.

[15] The choices we made for the following parameters have been dictated by the technical literature on OFDM-based JCAS systems (e.g., see [41]).

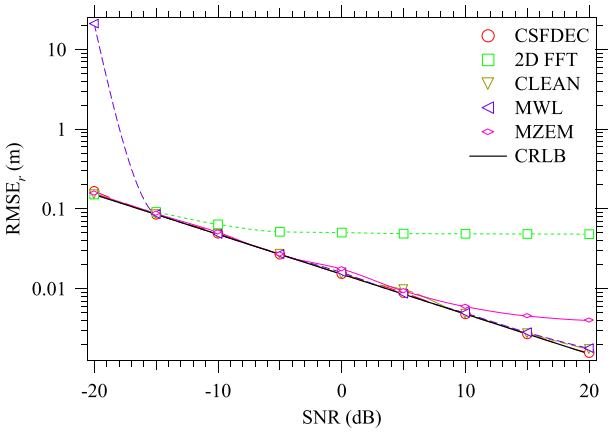

FIGURE 4. Root mean square error performance achieved in range estimation (second scenario) with $N = 256$ subcarriers. The 2D-FFT, CSFDEC, CLEAN, MWL and MZEM algorithms are considered.

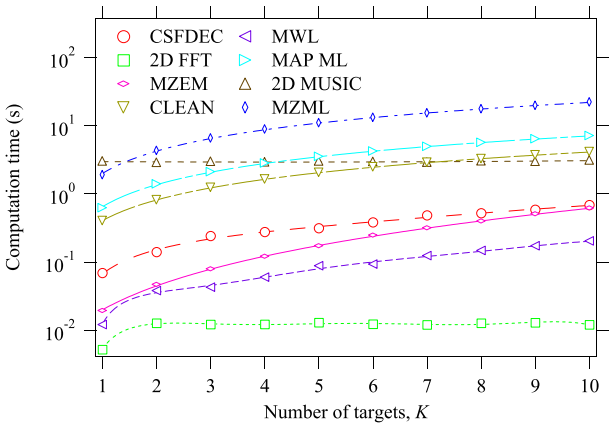

FIGURE 5. Computational time of the 2D-FFT, CSFDEC, CLEAN, MWL, 2D-MUSIC, MZML, MAP-ML and MZEM algorithms versus overall number of targets. The third scenario is considered.

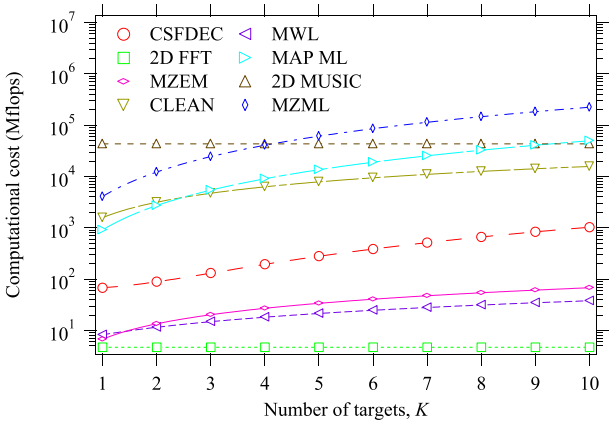

FIGURE 6. Estimated number of FLOPs of the 2D-FFT, CSFDEC, CLEAN, MWL, 2D-MUSIC, MZML, MAP-ML and MZEM algorithms versus overall number of targets (third scenario).

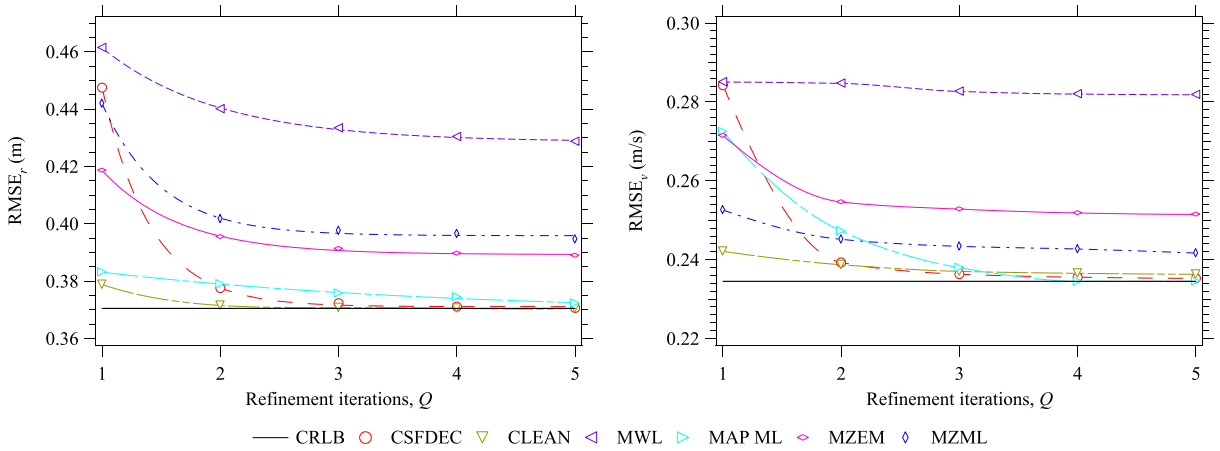

FIGURE 7. Root mean square error performance achieved in range and velocity estimation (fourth scenario). The CSFDEC, CLEAN, MWL, MZML, MAP-ML and MZEM algorithms are considered.

of the MZML, MAP-ML and MZEM algorithms; 3) in the CSFDEC algorithm, $N_{\text{it}} = 20$ refinement steps have been accomplished in the computation of the residuals and the interpolation[16] orders $I_D = I_r = 7$ have been selected; 4) a unit value has been assigned to the coefficient $\beta_k^{(i)}$ (with $k = 0, 1, \ldots, K-1$ and $i = 1, 2, \ldots, N_{\text{REF}}$) in the EM algorithm (see (91)); 5) $N_{\text{REF}} = 5$ ($N_{\text{REF}} = 3$) re-estimations have been executed by the CSFDEC, CLEAN and MWL (MZML, MAP-ML and MZEM) algorithms in the first three scenarios. Substantial attention has been paid to the selection of search grids. A brief description of the search grid adopted for the 2D-MUSIC is provided in Table 3, whereas that of the initial search grid employed for the CLEAN and MWL algorithms in Table 4. In both tables, the grid chosen for a specific scenario is described by the triplet $[X_{\min}, X_{\max}, Q_0]$, where $X_{\min}$ ($X_{\max}$) denotes the minimum (maximum) trial value for the variable X, and Q_0 represents the overall number of (uniformly spaced) trial values[17] ($Q = M$ if X represents the target range R, whereas $Q = N$ if X represents target velocity v). Moreover, in our simulations, $M_0 = N_0 = 11$ ($M_0 = N_0 = 9$) have been chosen for the grid size in the CLEAN and MWL (MZML, MAP-ML and MZEM) algorithms during the re-estimation steps. Some numerical results about the RMSE$_r$ and RMSE$_v$ characterizing all the considered algorithms in **S1** are illustrated in Fig. 2, where the *Cramer-Rao lower bound*[18] (CRLB) for the considered estimation problem is also shown. Note that: 1) most of the algorithms achieve poor estimation accuracy when the SNR drops below a threshold, which is algorithm dependent; 2) the threshold of the 2D-MUSIC, CLEAN and MWL algorithms is not visible in the considered SNR range; 3) the accuracy of each algorithm attains the CRLB above its SNR threshold, but, at high SNRs, may reach a floor. The last phenomenon, observed for the 2D-FFT and 2D-MUSIC algorithms, is due to their limited accuracy[19] (which depends on the overall number of FFT bins and on the overall number of trial points employed in the computation of the steering vectors, respectively). The other algorithms, instead, take advantage of their refinement cycles, which improve the accuracy of their final estimates.

In addition, in analyzing the results shown in Fig. 2, readers should keep in mind that: 1) the computational complexity of the CSFDEC, CLEAN and MZEM algorithms is approximately 13, 2.3 and 1.35 times higher, respectively, than that of the 2D-FFT, whereas that of the MWL algorithm is very close to it; 2) the complexity of the 2D-MUSIC, MAP-ML and MZML algorithms is 352, 183 and 819 times higher, respectively, than that of the 2D-FFT.

Most of the considerations illustrated above for Fig. 2 also apply to the results shown in Fig. 3 for $N = 32$ and in Fig. 4 for $N = 256$. In both cases **S2** is considered, but the results illustrated in Fig. 4 concern range estimation only and refer to a subset of the considered algorithms (2D-MUSIC, MZML and MAP-ML are ignored because of their huge memory requirements). Note that:

1) Unlike **S1**, an SNR threshold is visible in Fig. 3 for all the algorithms, mainly because of the presence of spectral leakage.

2) Independently of the considered algorithm, an higher number of subcarriers allows to achieve a lower RMSE$_r$ and reduce the SNR threshold.

3) In analyzing the results shown in Fig. 3, it should be kept into account that the computational complexity of the CSFDEC, CLEAN, MWL and MZEM algorithms is approximately 34, 177, 2.7 and 4.7 times higher, respectively, than that of the 2D-FFT. Moreover, the complexity of the

[16] In all our simulations, the *barycentric interpolation* technique described in [46] has been always used.

[17] This entails that the step size between adjacent trial values selected in the interval $[X_{\min}, X_{\max}]$ is $X_{\text{step}} = (X_{\max} - X_{\min})/(Q_0 - 1)$.

[18] The expression of the CRLB for range and velocity estimation in the case of single target can be found in [33, Appendix D]. The CRLB in the case of multiple targets, instead, can be easily derived following the procedure illustrated in [47].

[19] In the case of the 2D-FFT algorithm, this phenomenon can be mitigated by interpolating its cost function to improve the accuracy in peak detection.

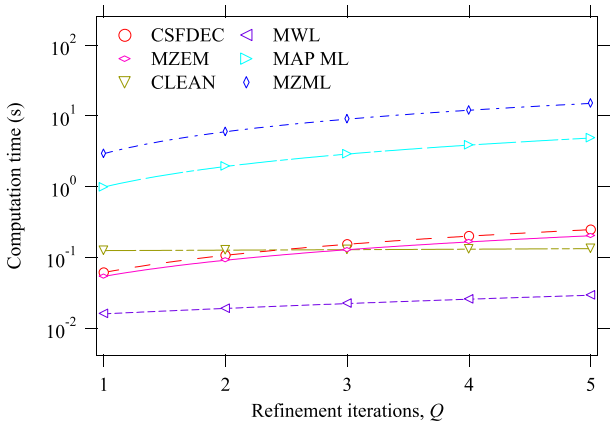

FIGURE 8. Computational time of the CSFDEC, CLEAN, MWL, MZML, MAP-ML and MZEM algorithms versus overall number of iterations (fourth scenario).

2D-MUSIC, MAP-ML and MZML algorithms is 7532, 1518 and 7070 times higher, respectively, than that of the 2D-FFT.

The CT[20] and the overall number of FLOPs assessed in **S3** are shown in Fig. 5 and Fig. 6, respectively. From these results and from those illustrated in **S1** and **S2**, it can be easily inferred that: 1) the gap, in terms of CT, between the CLEAN, MAP-ML and 2D-MUSIC algorithms is small; 2) the MAP-ML algorithm takes advantage of the *alternating projections* method to reduce the computational effort of the MZML algorithm; 3) the CT of the MWL algorithm is the closest to that of the 2D-FFT algorithm, but, as shown in Fig. 3, the former algorithm achieves a poorer estimation accuracy than the latter one for SNR $\in [-15, 3]$ dB; 4) the CSFDEC algorithm stays in the middle between high and low complexity algorithms, but is able to achieve excellent estimation accuracy, as evidenced by the RMSE results illustrated for the previous scenarios.

Some numerical results[21] referring to **S4** are shown in Fig. 7 for RMSE_r and RMSE_v and in Fig. 8 for the CT. These results deserve the following comments: 1) the estimation accuracy of most of the considered algorithms does not improve after the first three iterations; 2) the CLEAN, MZEM and CSFDEC algorithms exhibit similar CTs if three iterations are carried out for each of them; 3) the MWL algorithm requires a lower CT, but generates poorer range and velocity estimates.

V. CONCLUSION

In this manuscript, eight different algorithms for detecting multiple targets, and for jointly estimating their range and velocity in a SISO OFDM-based JCAS system have been described. All belong to the class of *indirect methods* and are deterministic; moreover, three of them (namely, the CLEAN, MWL and CSFDEC algorithms) exploit an iterative cancellation procedure in the estimation of target parameters. Our numerical results evidence that, in the presence of a single target or of multiple well spaced targets, all the considered algorithms achieve reasonable accuracy. However, their behavior substantially changes in the presence of multiple closely spaced targets; in such conditions, our attention has focused on how accuracy and computational effort are influenced by the overall number of a) targets and b) refinement cycles employed to improve the quality of the final estimates of target parameters. The following conclusions can be formulated in the light of our simulation results: 1) the CLEAN and CSFDEC algorithms require a limited complexity and achieve excellent performance thanks to the use of a target cancellation procedure; 2) the MZML and MAP-ML algorithms achieve better accuracy than subspace-based method (i.e., than the 2D MUSIC algorithm) at the price of similar (and really high) computational complexities; 3) the MWL algorithm achieves a better accuracy-complexity trade-off than the MAP-ML algorithm. Therefore, in future OFDM-based JCAS system, the selection of a target detection and estimation algorithm requires a careful assessment of the pros and cons characterizing the various options available in the technical literature. Our ongoing work concerns the possible extensions of the considered algorithms to MIMO OFDM-based radars.

[20]The values shown for this parameter represent averages computed over one thousand runs for each algorithm.

[21]Please note that a linear scale is adopted on the ordinate axis of Fig. 7, since the interval which the estimated RMSEs belong to is narrow.

REFERENCES

[1] P. Kumari, J. Choi, N. González-Prelcic, and R. W. Heath, "IEEE 802.11ad-based radar: An approach to joint vehicular communication-radar system," *IEEE Trans. Veh. Technol.*, vol. 67, no. 4, pp. 3012–3027, Apr. 2018.

[2] G. Duggal, S. Vishwakarma, K. V. Mishra, and S. S. Ram, "Doppler-resilient 802.11ad-based ultrashort range automotive joint radar-communications system," *IEEE Trans. Aerosp. Electron. Syst.*, vol. 56, no. 5, pp. 4035–4048, Oct. 2020.

[3] R. C. Daniels, E. R. Yeh, and R. W. Heath, "Forward collision vehicular radar with IEEE 802.11: Feasibility demonstration through measurements," *IEEE Trans. Veh. Technol.*, vol. 67, no. 2, pp. 1404–1416, Feb. 2018.

[4] K. V. Mishra, M. R. B. Shankar, V. Koivunen, B. Ottersten, and S. A. Vorobyov, "Toward millimeter-wave joint radar communications: A signal processing perspective," *IEEE Signal Process. Mag.*, vol. 36, no. 5, pp. 100–114, Sep. 2019.

[5] J. A. Zhang, F. Liu, C. Masouros, R. W. Heath, Z. Feng, L. Zheng, and A. Petropulu, "An overview of signal processing techniques for joint communication and radar sensing," *IEEE J. Sel. Topics Signal Process.*, vol. 15, no. 6, pp. 1295–1315, Nov. 2021.

[6] Md. L. Rahman, J. A. Zhang, X. Huang, Y. J. Guo, and R. W. Heath, "Framework for a perceptive mobile network using joint communication and radar sensing," *IEEE Trans. Aerosp. Electron. Syst.*, vol. 56, no. 3, pp. 1926–1941, Jun. 2020.

[7] J. A. Zhang, A. Cantoni, X. Huang, Y. J. Guo, and R. W. Heath, "Framework for an innovative perceptive mobile network using joint communication and sensing," in *Proc. IEEE 85th Veh. Technol. Conf. (VTC Spring)*, Jun. 2017, pp. 1–5.

[8] J. A. Zhang, X. Huang, Y. J. Guo, and Md. L. Rahman, "Signal stripping based sensing parameter estimation in perceptive mobile networks," in *Proc. IEEE-APS Topical Conf. Antennas Propag. Wireless Commun. (APWC)*, Sep. 2017, pp. 67–70.

[9] L. Zheng and X. Wang, "Super-resolution delay-Doppler estimation for OFDM passive radar," *IEEE Trans. Signal Process.*, vol. 65, no. 9, pp. 2197–2210, May 2017.

[10] C. Sturm and W. Wiesbeck, "Waveform design and signal processing aspects for fusion of wireless communications and radar sensing," *Proc. IEEE*, vol. 99, no. 7, pp. 1236–1259, Jul. 2011.
[11] G. Hakobyan and B. Yang, "High-performance automotive radar: A review of signal processing algorithms and modulation schemes," *IEEE Signal Process. Mag.*, vol. 36, no. 5, pp. 32–44, Sep. 2019.
[12] L. Zheng, M. Lops, Y. C. Eldar, and X. Wang, "Radar and communication coexistence: An overview: A review of recent methods," *IEEE Signal Process. Mag.*, vol. 36, no. 5, pp. 85–99, Sep. 2019.
[13] A. Hassanien, M. G. Amin, E. Aboutanios, and B. Himed, "Dual-function radar communication systems: A solution to the spectrum congestion problem," *IEEE Signal Process. Mag.*, vol. 36, no. 5, pp. 115–126, Sep. 2019.
[14] F. Liu, C. Masouros, A. P. Petropulu, H. Griffiths, and L. Hanzo, "Joint radar and communication design: Applications, state-of-the-art, and the road ahead," *IEEE Trans. Commun.*, vol. 68, no. 6, pp. 3834–3862, Jun. 2020.
[15] Z. Feng, Z. Fang, Z. Wei, X. Chen, Z. Quan, and D. Ji, "Joint radar and communication: A survey," *China Commun.*, vol. 17, no. 1, pp. 1–27, Jan. 2020.
[16] D. Ma, N. Shlezinger, T. Huang, Y. Liu, and Y. C. Eldar, "Joint radar-communication strategies for autonomous vehicles: Combining two key automotive technologies," *IEEE Signal Process. Mag.*, vol. 37, no. 4, pp. 85–97, Jul. 2020.
[17] T. Wild, V. Braun, and H. Viswanathan, "Joint design of communication and sensing for beyond 5G and 6G systems," *IEEE Access*, vol. 9, pp. 30845–30857, 2021.
[18] L. G. De Oliveira, B. Nuss, M. B. Alabd, A. Diewald, M. Pauli, and T. Zwick, "Joint radar-communication systems: Modulation schemes and system design," *IEEE Trans. Microw. Theory Techn.*, vol. 70, no. 3, pp. 1521–1551, Mar. 2022.
[19] J. A. Zhang, M. L. Rahman, K. Wu, X. Huang, Y. J. Guo, S. Chen, and J. Yuan, "Enabling joint communication and radar sensing in mobile networks—A survey," *IEEE Commun. Surveys Tuts.*, vol. 24, no. 1, pp. 306–345, 1st Quart., 2022.
[20] C. R. Berger, B. Demissie, J. Heckenbach, P. Willett, and S. Zhou, "Signal processing for passive radar using OFDM waveforms," *IEEE J. Sel. Topics Signal Process.*, vol. 4, no. 1, pp. 226–238, Feb. 2010.
[21] D. Roque and S. Bidon, "Range migration in symbol-based OFDM radar receivers," in *Proc. IEEE 22nd Int. Workshop Signal Process. Adv. Wireless Commun. (SPAWC)*, Sep. 2021, pp. 496–500.
[22] C. F. Van Loan and G. Golub, "Matrix computations," in *Matrix Computations*, vol. 53. Baltimore, MD, USA: The Johns Hopkins Univ. Press, 1996.
[23] P. Di Viesti, A. Davoli, G. Guerzoni, and G. M. Vitetta, "Novel methods for approximate maximum likelihood estimation of multiple superimposed undamped tones and their application to radar systems," TechRxiv, Aug. 2021, doi: 10.36227/techrxiv.15054321.v2.
[24] S. Mercier, S. Bidon, D. Roque, and C. Enderli, "Comparison of correlation-based OFDM radar receivers," *IEEE Trans. Aerosp. Electron. Syst.*, vol. 56, no. 6, pp. 4796–4813, Dec. 2020.
[25] X. Liu, T. Zhang, Q. Shi, and L. Kong, "CP-OFDM radar range reconstruction in a chaotic Doppler disturbed scenario," in *Proc. IEEE Radar Conf.*, Sep. 2020, pp. 1–5.
[26] Y. L. Sit, C. Sturm, and T. Zwick, "Doppler estimation in an OFDM joint radar and communication system," in *Proc. German Microw. Conf.*, Mar. 2011, pp. 1–4.
[27] S. Mercier, D. Roque, and S. Bidon, "Study of the target self-interference in a low-complexity OFDM-based radar receiver," *IEEE Trans. Aerosp. Electron. Syst.*, vol. 55, no. 3, pp. 1200–1212, Jun. 2019.
[28] G. Liu, H. Niu, M. Zheng, D. Bao, J. Cai, G. Qin, B. Wu, P. Li, and N. Liu, "Integration of communication and SAR radar based on OFDM with channel estimation in high speed scenario," in *Proc. IEEE Int. Geosci. Remote Sens. Symp.*, Yokohama, Japan, Jul. 2019, pp. 2519–2522.
[29] Y. Zeng, Y. Ma, and S. Sun, "Joint radar-communication: Low complexity algorithm and self-interference cancellation," in *Proc. IEEE Global Commun. Conf. (GLOBECOM)*, Dec. 2018, pp. 1–7.
[30] J. B. Sanson, D. Castanheira, A. Gameiro, and P. P. Monteiro, "Fusion of radar and communication information for tracking in OFDM automotive radar at 24 GHz," in *IEEE MTT-S Int. Microw. Symp. Dig.*, Los Angeles, CA, USA, Aug. 2020, pp. 1153–1156.
[31] S. Schieler, C. Schneider, C. Andrich, M. Döbereiner, J. Luo, A. Schwind, R. S. Thomä, and G. Del Galdo, "OFDM waveform for distributed radar sensing in automotive scenarios," *Int. J. Microw. Wireless Technol.*, vol. 12, no. 8, pp. 716–722, Oct. 2020.
[32] S. Mercier, D. Roque, S. Bidon, and C. Enderli, "Correlation-based radar receivers with pulse-shaped OFDM signals," in *Proc. IEEE Radar Conf.*, Florence, Italy, Sep. 2020, pp. 1–6.
[33] M. Mirabella, P. Di Viesti, A. Davoli, and G. M. Vitetta, "An approximate maximum likelihood method for the joint estimation of range and Doppler of multiple targets in OFDM-based radar systems," *IEEE Trans. Commun.*, 2023, doi: 10.1109/TCOMM.2023.3280562.
[34] J. Tsao and B. D. Steinberg, "Reduction of sidelobe and speckle artifacts in microwave imaging: The CLEAN technique," *IEEE Trans. Antennas Propag.*, vol. 36, no. 4, pp. 543–556, Apr. 1988.
[35] A. Davoli, E. Sirignano, and G. M. Vitetta, "Three-dimensional deterministic detection and estimation algorithms for MIMO SFCW radars," in *Proc. IEEE Radar Conf.*, Florence, Italy, Sep. 2020, pp. 1–6.
[36] E. Sirignano, A. Davoli, G. M. Vitetta, and F. Viappiani, "A comparative analysis of deterministic detection and estimation techniques for MIMO SFCW radars," *IEEE Access*, vol. 7, pp. 129848–129861, 2019.
[37] R. Xie, D. Hu, K. Luo, and T. Jiang, "Performance analysis of joint range-velocity estimator with 2D-MUSIC in OFDM radar," *IEEE Trans. Signal Process.*, vol. 69, pp. 4787–4800, 2021.
[38] D. H. N. Nguyen and R. W. Heath, "Delay and Doppler processing for multi-target detection with IEEE 802.11 OFDM signaling," in *Proc. IEEE Int. Conf. Acoust., Speech Signal Process. (ICASSP)*, Mar. 2017, pp. 3414–3418.
[39] Y. Liu, G. Liao, Y. Chen, J. Xu, and Y. Yin, "Super-resolution range and velocity estimations with OFDM integrated radar and communications waveform," *IEEE Trans. Veh. Technol.*, vol. 69, no. 10, pp. 11659–11672, Oct. 2020.
[40] A. Jakobsson, A. L. Swindlehurst, and P. Stoica, "Subspace-based estimation of time delays and Doppler shifts," *IEEE Trans. Signal Process.*, vol. 46, no. 9, pp. 2472–2483, Sep. 1998.
[41] F. Zhang, Z. Zhang, W. Yu, and T. Truong, "Joint range and velocity estimation with intrapulse and intersubcarrier Doppler effects for OFDM-based RadCom systems," *IEEE Trans. Signal Process.*, vol. 68, pp. 662–675, 2020.
[42] U. K. Singh, R. Mitra, V. Bhatia, and A. K. Mishra, "Target range estimation in OFDM radar system via kernel least mean square technique," in *Proc. Int. Conf. Radar Syst.*, Oct. 2017, pp. 1–5.
[43] U. K. Singh, V. Bhatia, and A. K. Mishra, "Delay and Doppler shift estimation for non-constant envelope modulation in OFDM radar system," in *Proc. Int. Conf. Radar Syst.* Belfast, U.K.: Institution of Engineering and Technology, Oct. 2017, pp. 1–5.
[44] A. El Assaad, M. Krug, and G. Fischer, "Distance and vehicle speed estimation in OFDM multipath channels," in *Proc. 21st Int. Conf. Microw., Radar Wireless Commun. (MIKON)*, May 2016, pp. 1–5.
[45] T. K. Moon, "The expectation-maximization algorithm," *IEEE Signal Process. Mag.*, vol. 13, no. 6, pp. 47–60, Nov. 1997.
[46] J.-P. Berrut and L. N. Trefethen, "Barycentric Lagrange interpolation," *SIAM Rev.*, vol. 46, no. 3, pp. 501–517, Jan. 2004.
[47] Y.-X. Yao and S. M. Pandit, "Cramér-Rao lower bounds for a damped sinusoidal process," *IEEE Trans. Signal Process.*, vol. 43, no. 4, pp. 878–885, Apr. 1995.

MICHELE MIRABELLA (Graduate Student Member, IEEE) received the B.S. and M.S. degrees (cum laude) in electronic engineering from the University of Modena and Reggio Emilia, Italy, in 2019 and 2021, respectively, where he is currently pursuing the Ph.D. degree. His main research interests include joint communication and sensing systems.

PASQUALE DI VIESTI (Graduate Student Member, IEEE) received the bachelor's and master's degrees (cum laude) in electronic engineering from the University of Modena and Reggio Emilia, Italy, in 2016 and 2018, respectively, and the Ph.D. degree in automotive for an intelligent mobility from the University of Bologna, in 2021. He is currently a Postdoctoral Research Fellow with the University of Modena and Reggio Emilia. His main research interests include statistical signal processing and MIMO radars.

ALESSANDRO DAVOLI (Graduate Student Member, IEEE) received the B.S. and M.S. degrees (cum laude) in electronic engineering from the University of Modena and Reggio Emilia, Italy, in 2016 and 2018, respectively, and the Ph.D. degree in automotive for an intelligent mobility from the University of Bologna, in October 2021. His main research interests include MIMO radars, with emphasis on the development of novel detection and estimation algorithms for automotive applications.

GIORGIO M. VITETTA (Senior Member, IEEE) received the Dr.Ing. degree (cum laude) in electronic engineering and the Ph.D. degree from the University of Pisa, Italy, in 1990 and 1994, respectively. He has been a Full Professor of telecommunications with the University of Modena and Reggio Emilia, since 2001. He has coauthored more than 100 papers published on international journals and on the proceedings of international conferences, and has coauthored the book titled *Wireless Communications: Algorithmic Techniques* (John Wiley, 2013). His main research interests include the broad areas of wireless and wired data communications, localization systems, MIMO radars, and the smart grids. He has served as an Area Editor for the IEEE TRANSACTIONS ON COMMUNICATIONS and an Associate Editor for the IEEE WIRELESS COMMUNICATIONS LETTERS and the IEEE TRANSACTIONS ON WIRELESS COMMUNICATIONS.

Open Access funding provided by 'Università degli Studi di Modena e Reggio Emilia' within the CRUI CARE Agreement